Available online at www.sciencedirect.com
SCIENCE DIRECT®
C. R. Physique 6 (2005) 467–486
COMPTES RENDUS PHYSIQUE
http://france.elsevier.com/direct/COMREN/

Aircraft trailing vortices/Tourbillons de sillages d'avions

Vortex methods and their application to trailing wake vortex simulations

Grégoire Winckelmans *, Roger Cocle, Louis Dufresne, Raphaël Capart

Université catholique de Louvain (UCL), Mechanical Engineering Department, Division TERM and Center for Systems Engineering and Applied Mechanics (CESAME), 1348 Louvain-la-Neuve, Belgium

Available online 5 July 2005

Abstract

Vortex methods are competitive for simulating incompressible unsteady flows, because they have negligible dispersion error and good energy conservation. The various methods are presented, including the recent developments: particle redistribution, diffusion, relaxation (by projection), efficient solvers (fast multipole method, vortex-in-cell method, hybrid method) and parallel computer implementations. Examples relating to wing/aircraft trailing wake vortices are presented: 2-D and 3-D, inviscid and viscous, direct numerical simulation and large eddy simulation. We consider wake roll-ups, vortex tube dynamics, 3-D instabilities and the complexity/turbulence they produce. A vortex system in ground effects is also presented. ***To cite this article: G. Winckelmans et al., C. R. Physique 6 (2005).***

Résumé

Les méthodes vortex et leur application à la simulation des sillages tourbillonnaires. Les méthodes vortex sont compétitives pour la simulation d'écoulements incompressibles et instationnaires, car elles ont peu de dispersion et de bonnes propriétés de conservation de l'énergie. Les diverses méthodes sont présentées, incluant les développements récents : redistribution des particules, diffusion, relaxation (par projection), solveurs efficaces (méthode multipole rapide, méthode particules-grille, méthode hybride) et implémentation sur ordinateurs parallèles. Des examples sont présentés concernant l'application aux sillages tourbillonnaires d'ailes/avions : 2-D et 3-D, non-visqueux et visqueux, simulation directe et simulation des grandes échelles. On considère des enroulements, de la dynamique de tubes tourbillon, des instabilités 3-D et la complexité/turbulence qu'elles produisent. Un système de tourbillons en effet de sol est aussi présenté. ***Pour citer cet article : G. Winckelmans et al., C. R. Physique 6 (2005).***

Keywords: Lagrangian methods; Vortex particle methods; Vortex-in-cell methods; Unsteady flows; Turbulent flows; Direct numerical simulation; Large-eddy simulation

Mots-clés : Méthodes lagrangiennes ; Méthodes de particules tourbillon ; Méthodes particules-grille ; Écoulements instationnaires ; Écoulements turbulents ; Simulation numérique directe ; Simulation des grandes échelles

* Corresponding author.
E-mail address: winckelmans@term.ucl.ac.be (G. Winckelmans).

1631-0705/$ – see front matter
doi:10.1016/j.crhy.2005.05.001

1. Introduction

This paper presents vortex methods and their application to the simulation of wing/aircraft trailing wake vortices. Vortex methods are Lagrangian methods used to simulate unsteady convection-dominated problems. Since they are Lagrangian, they have negligible dispersion error. They also have good energy conservation properties. These two qualities make them efficient tools for the simulation of convection dominated flows: direct numerical simulations (DNS) and large-eddy simulations (LES). Recent and global references on vortex methods can be found in [1,2,35].

We define the velocity $\mathbf{u}$, the *material derivative* $\frac{Df}{Dt} \triangleq \frac{\partial f}{\partial t} + (\nabla f)\cdot\mathbf{u}$ and the *conservative derivative* $\frac{\mathcal{D}f}{\mathcal{D}t} \triangleq \frac{\partial f}{\partial t} + \nabla\cdot(f\mathbf{u})$. They are related by $\frac{\mathcal{D}f}{\mathcal{D}t} = \frac{Df}{Dt} + f\nabla\cdot\mathbf{u}$. The conservation of mass is $\frac{\mathcal{D}\rho}{\mathcal{D}t} = 0$ or, equivalently, $\frac{D\rho}{Dt} = -\rho\nabla\cdot\mathbf{u}$. This leads to the property $\rho\frac{Df}{Dt} = \frac{\mathcal{D}}{\mathcal{D}t}(\rho f)$. Considering $f(\mathbf{x},t)$ integrated over a small material volume $V(t)$ and using Leibnitz theorem, one obtains

$$\frac{\mathrm{d}}{\mathrm{d}t}\int\limits_{V(t)} f\,\mathrm{d}\mathbf{x} = \int\limits_{V(t)} \frac{\partial f}{\partial t}\,\mathrm{d}\mathbf{x} + \int\limits_{S(t)} f\mathbf{u}\cdot\mathbf{n}\,\mathrm{d}\mathbf{x} = \int\limits_{V(t)} \left(\frac{\partial f}{\partial t} + \nabla\cdot(f\mathbf{u})\right)\mathrm{d}\mathbf{x} = \int\limits_{V(t)} \frac{\mathcal{D}f}{\mathcal{D}t}\,\mathrm{d}\mathbf{x} \tag{1}$$

Lagrangian methods follow the evolution of quantities integrated over material volumes. The physical field f is discretized using *particles*. Each p particle represents a small material volume V_p. The *strength* of each particle represents the integral of f over the material volume: $\alpha_p = \int_{V_p} f\,\mathrm{d}\mathbf{x} \triangleq f_p V_p$. The *position* (centroid) of each material volume is denoted by $\mathbf{x}_p$. Each material volume is carried by the local velocity field: $\mathbf{u}_p = \mathbf{u}(\mathbf{x}_p(t),t)$. Its strength evolves according to the discretized version of Eq. (1). Its volume evolves according to the conservation of mass: $\frac{\mathrm{d}}{\mathrm{d}t}(\rho V)_p = 0$ and thus $\frac{1}{V_p}\frac{\mathrm{d}V_p}{\mathrm{d}t} = -\frac{1}{\rho_p}\frac{\mathrm{d}\rho_p}{\mathrm{d}t} = (\nabla\cdot\mathbf{u})_p$. In summary, one obtains:

$$\frac{\mathrm{d}}{\mathrm{d}t}\mathbf{x}_p = \mathbf{u}_p, \qquad \frac{\mathrm{d}}{\mathrm{d}t}(f_p V_p) = \left(\frac{\mathcal{D}f}{\mathcal{D}t}\right)_p V_p, \qquad \frac{\mathrm{d}}{\mathrm{d}t}V_p = (\nabla\cdot\mathbf{u})_p V_p \tag{2}$$

This defines the method. It is thus a method which is simply the Lagrangian expression of the conservation equation considered.

We here focus on the methods used to solve the vorticity formulation of the Navier–Stokes equations for incompressible ($\nabla\cdot\mathbf{u} = 0$) and viscous flows of Newtonian fluids. The equation for the evolution of the vorticity, $\boldsymbol{\omega} = \nabla\times\mathbf{u}$, is obtained by taking the curl of the momentum equation:

$$\frac{D\boldsymbol{\omega}}{Dt} - \nu\nabla^2\boldsymbol{\omega} = (\nabla\mathbf{u})\cdot\boldsymbol{\omega} \equiv (\nabla\mathbf{u})^{\mathrm{T}}\cdot\boldsymbol{\omega} \equiv \mathbf{S}\cdot\boldsymbol{\omega} = \nabla\cdot(\mathbf{u}\boldsymbol{\omega}) \tag{3}$$

where ν is the kinematic viscosity, $\nabla^2\boldsymbol{\omega}$ stands for $\nabla\cdot(\nabla\boldsymbol{\omega})$ (a notation used throughout) and $\mathbf{S} = \frac{1}{2}(\nabla\mathbf{u} + (\nabla\mathbf{u})^{\mathrm{T}})$ is the strain rate tensor. The forms of the stretching term are equivalent because of the identity $((\nabla\mathbf{a}) - (\nabla\mathbf{a})^{\mathrm{T}})\cdot\mathbf{b} = (\nabla\times\mathbf{a})\times\mathbf{b}$.

Recalling the evolution equation for a differential material element, $\frac{D}{Dt}\delta\mathbf{l} = (\nabla\mathbf{u})\cdot\delta\mathbf{l}$, one concludes that, in 3-D inviscid flows, a *vortex line* (line everywhere tangent to the local vorticity) moves as a material line; consequently, a *vortex tube* (tube made of an ensemble of vortex lines) moves as a material tube: this property forms the basis of the *method of vortex filaments*.

The velocity is obtained as $\mathbf{u} = \nabla\times\boldsymbol{\psi} + \mathbf{u}_p$, with $\mathbf{u}_p$ a potential velocity (e.g., a uniform free stream velocity) and $\boldsymbol{\psi}$ the streamfunction related to $\boldsymbol{\omega}$ by a Poisson equation: $\nabla^2\boldsymbol{\psi} = -\boldsymbol{\omega}$.

In 2-D flows, the vorticity only has one component (perpendicular to the velocity field), hence no vorticity stretching: $\boldsymbol{\omega} = \omega\mathbf{e}_z$ with $\omega = \frac{\partial v}{\partial x} - \frac{\partial u}{\partial y}$. The streamfunction also has one component: $\boldsymbol{\psi} = \psi\mathbf{e}_z$, $u = \frac{\partial\psi}{\partial y}$, $v = -\frac{\partial\psi}{\partial x}$, also leading to $\nabla^2\psi = -\omega$. The vorticity equation reduces to

$$\frac{D\omega}{Dt} = \nu\nabla^2\omega \tag{4}$$

The streamfunction (and thus the velocity) are obtained using either a Green's function approach (Biot–Savart, as in the *fast multipole method*) or a fast Poisson solver on a grid (as in the *vortex-in-cell method*, VIC). With the Green's function approach, one has (3-D and 2-D respectively):

$$\boldsymbol{\psi}(\mathbf{x}) = \frac{1}{4\pi}\int \frac{1}{|\mathbf{x}-\mathbf{x}'|}\boldsymbol{\omega}(\mathbf{x}')\,\mathrm{d}\mathbf{x}', \qquad \psi(\mathbf{x}) = \frac{1}{2\pi}\int \log\left(\frac{L}{|\mathbf{x}-\mathbf{x}'|}\right)\omega(\mathbf{x}')\,\mathrm{d}\mathbf{x}' \tag{5}$$

with L any reference length (ψ defined up to a constant). The induced velocity is then:

$$\mathbf{u}(\mathbf{x}) = -\frac{1}{4\pi}\int \frac{(\mathbf{x}-\mathbf{x}')}{|\mathbf{x}-\mathbf{x}'|^3}\times\boldsymbol{\omega}(\mathbf{x}')\,\mathrm{d}\mathbf{x}', \qquad \mathbf{u}(\mathbf{x}) = -\frac{1}{2\pi}\int \frac{(\mathbf{x}-\mathbf{x}')}{|\mathbf{x}-\mathbf{x}'|^2}\times\big(\omega(\mathbf{x}')\mathbf{e}_z\big)\,\mathrm{d}\mathbf{x}' \tag{6}$$

There are also fundamental invariants and/or diagnostics for 2-D and 3-D unbounded flows: see [3] (and also [1,2] in the context of vortex methods).

2. 2-D vortex methods

The 2-D *method of regularized vortex particles* (also called *vortex blobs*) is first considered (the singular method being not very practical, see [1,2]). One associates to each particle an area S_p and a *circulation* Γ_p, the integral of ω over the material surface: $\Gamma_p = \int_{S_p} \omega dS \stackrel{\triangle}{=} \omega_p S_p$. The method reads

$$\frac{\mathrm{d}}{\mathrm{d}t}\mathbf{x}_p = \mathbf{u}_p, \qquad \frac{\mathrm{d}}{\mathrm{d}t}\Gamma_p = \big(\nu\nabla^2\omega\big)_p S_p \tag{7}$$

The induced velocity field is determined by using a regularized Biot–Savart integral. The simplest is to use radially symmetric regularization functions:

$$\mathbf{u}_\sigma(\mathbf{x}) = -\frac{1}{2\pi}\sum_p \frac{g_\sigma(|\mathbf{x}-\mathbf{x}_p|)}{|\mathbf{x}-\mathbf{x}_p|^2}(\mathbf{x}-\mathbf{x}_p)\times(\Gamma_p\mathbf{e}_z) \tag{8}$$

with σ the regularization length and $g_\sigma(r) \stackrel{\triangle}{=} g(\frac{r}{\sigma})$ the regularization function, with $g(\rho)\to 1$ for $\rho \stackrel{\triangle}{=} \frac{r}{\sigma}$ large and $g(\rho)\propto\rho^2$ for ρ small. The self-induced velocity is $u_\theta(r) = \frac{\Gamma}{2\pi}\frac{g(r/\sigma)}{r}$. The corresponding streamfunction is then obtained as

$$\psi_\sigma(\mathbf{x}) = -\frac{1}{2\pi}\sum_p G_\sigma\big(|\mathbf{x}-\mathbf{x}_p|\big)\Gamma_p \tag{9}$$

with $G_\sigma(r) \stackrel{\triangle}{=} G(\frac{r}{\sigma})$ and $\frac{g(\rho)}{\rho^2} = \frac{1}{\rho}\frac{\mathrm{d}G}{\mathrm{d}\rho}(\rho)$. This streamfunction also corresponds to the solution of $\nabla^2\psi_\sigma = -\omega_\sigma$ with

$$\omega_\sigma(\mathbf{x}) = \zeta_\sigma * \omega_\delta = \sum_p \zeta_\sigma\big(|\mathbf{x}-\mathbf{x}_p|\big)\Gamma_p \tag{10}$$

where $\zeta_\sigma(|\mathbf{x}|) \stackrel{\triangle}{=} \frac{1}{2\pi\sigma^2}\zeta(\frac{r}{\sigma})$ and $\zeta(\rho) = \frac{1}{\rho}\frac{\mathrm{d}}{\mathrm{d}\rho}\big(\rho\frac{\mathrm{d}G}{\mathrm{d}\rho}(\rho)\big)$. On also obtains $\zeta(\rho) = \frac{1}{\rho}\frac{\mathrm{d}g}{\mathrm{d}\rho}(\rho)$ and thus $g(\rho) = \int_0^\rho \zeta(s)s\,\mathrm{d}s$. The streamfunction and the velocity field are thus those induced by the particles considered as *vortex blobs*, the blob function being $\zeta_\sigma(r)$ with σ the characteristic size. The normalization, $\int\zeta_\sigma(|\mathbf{x}|)\,\mathrm{d}\mathbf{x} = 1$, leads to $\int_0^\infty \zeta(\rho)\rho\,\mathrm{d}\rho = 1$ (consistent with $g\to 1$ as $\rho\to\infty$). The inviscid version of the method is thus

$$\frac{\mathrm{d}}{\mathrm{d}t}\mathbf{x}_p = -\frac{1}{2\pi}\sum_q \frac{g_\sigma(|\mathbf{x}_p-\mathbf{x}_q|)}{|\mathbf{x}_p-\mathbf{x}_q|^2}(\mathbf{x}_p-\mathbf{x}_q)\times(\Gamma_p\mathbf{e}_z) \tag{11}$$

It conserves the impulse $\mathbf{I} = \sum_p \mathbf{x}_p\times(\Gamma_p\mathbf{e}_z)$ and the angular impulse $A = -\frac{1}{2}\sum_p|\mathbf{x}_p|^2\Gamma_p$. It also conserves the energy,

$$E = \frac{1}{2}\sum_p \Gamma_p\psi_\sigma(\mathbf{x}_p) = -\frac{1}{4\pi}\sum_{p,q}\Gamma_p G_\sigma\big(|\mathbf{x}_p-\mathbf{x}_q|\big)\Gamma_q \tag{12}$$

The viscous version of the method is obtained when one adds a diffusion scheme, such as the PSE (see later and Eq. (31)). The methods converge for regular vorticity fields as the number of particles is increased provided that the cores of neighbor blobs maintain overlapping (defining $S \stackrel{\triangle}{=} h^2$ for the fluid area of each particle, one requires that $\sigma/h \geqslant 1$) and that *particle redistribution schemes* are used (see later).

In general, a function is said to be of order r (here 'order' refers to spatial truncation error) when it satisfies the moment properties $\int x_1^{p_1}x_2^{p_2}\zeta_\sigma(\mathbf{x})\,\mathrm{d}\mathbf{x} = 0$ if $1\leqslant p_1+p_2<r$ and $\int|\mathbf{x}|^r|\zeta_\sigma(\mathbf{x})|\,\mathrm{d}\mathbf{x}<\infty$. Order higher than $r=2$ calls for functions that are not strictly positive. For radially symmetric functions, these become $\int_0^\infty\zeta(\rho)\rho^{1+s}\,\mathrm{d}\rho = 0$ for s even and $2\leqslant s<r$, and $\int_0^\infty|\zeta(\rho)|\rho^{1+r}\,\mathrm{d}\rho<\infty$ (see, e.g., [4] for a review list of functions, and Table 1 for usual ones). The *low order algebraic* function has $r=0$: it can only be used for global vortex modelling, as it does not converge for detailed field discretizations. For detailed studies, we typically use $r=2$ functions: the *high order algebraic* function or the *Gaussian* function. The $r=4$ functions are not strictly positive; in principle, they lead to a 4th order method (we have no experience in using them).

The vortex method can also be used with σ different for each particle (see also [32] and later for the method with non-uniform spatial resolution, $S_p \stackrel{\triangle}{=} h_p^2$, but that varies slowly in space). One then uses the symmetrized version (replace σ^2 by $\sigma_{pq}^2 \stackrel{\triangle}{=} \frac{1}{2}(\sigma_p^2+\sigma_q^2)$ in the dynamics of Eq. (11)), which ensures the conservation of impulse, angular impulse and energy. For viscous flows, one uses the symmetrized PSE scheme (see later).

The 2-D method, when combined with particle redistribution and with efficient velocity evaluation (see later) has a wide range of applicability: inviscid and viscous flows. It is comparable to most 2-D Eulerian methods of quality used to solve convection–diffusion problems, eventually with source terms.

Table 1
Examples of 2-D regularization functions

Function	$g(\rho)$	$G(\rho)$	$\zeta(\rho)$	r
Low order algebraic	$\frac{\rho^2}{\rho^2+1}$	$\frac{1}{2}\log(\rho^2+1)$	$\frac{2}{(\rho^2+1)^2}$	0
High order algebraic	$\frac{\rho^2(\rho^2+2)}{(\rho^2+1)^2}$	$\frac{1}{2}[\log(\rho^2+1)+\frac{\rho^2}{\rho^2+1}]$	$\frac{4}{(\rho^2+1)^3}$	2
Gaussian	$1-\mathrm{e}^{-\rho^2/2}$	$\frac{1}{2}[\log(\frac{\rho^2}{2})+\mathrm{E}_1(\frac{\rho^2}{2})]$	$\mathrm{e}^{-\rho^2/2}$	2
Super-Gaussian	$1-(1-\frac{\rho^2}{2})\mathrm{e}^{-\rho^2/2}$	$\frac{1}{2}[\log(\frac{\rho^2}{2})+\mathrm{E}_1(\frac{\rho^2}{2})-\mathrm{e}^{-\rho^2/2}]$	$(2-\frac{\rho^2}{2})\mathrm{e}^{-\rho^2/2}$	4

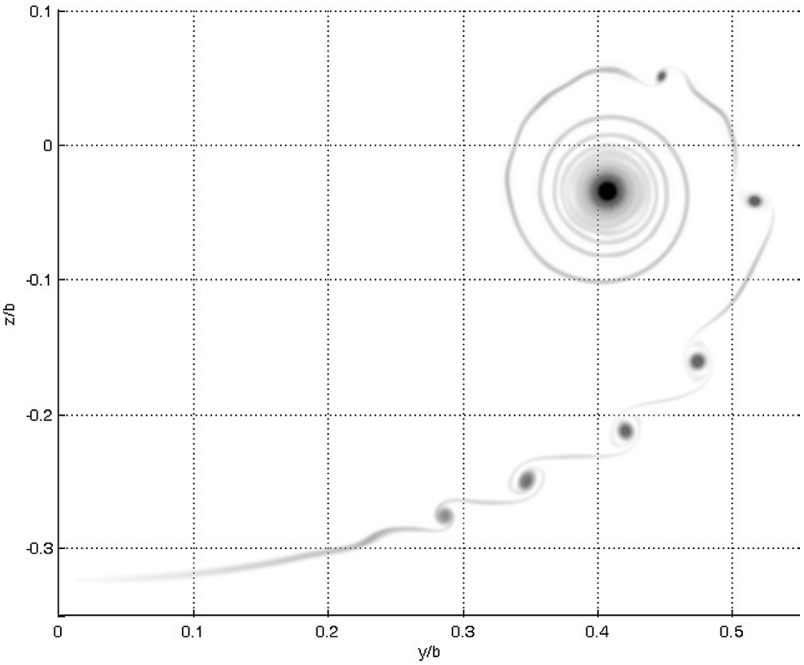

Fig. 1. Example of roll-up of a thin vortex sheet corresponding to an airfoil with elliptical loading. Vorticity field at $\tau = 0.10$.

An illustrative example, obtained using the inviscid version of the method, is presented in Fig. 1. This corresponds to the 2-D roll-up of a thin vortex sheet emitted by an airfoil. Its circulation per unit length is $\gamma(y) = -\frac{\mathrm{d}\Gamma}{\mathrm{d}y}(y)$ with $\Gamma(y) = \Gamma_0[1 - y^2/(b/2)^2]^{1/2}$ (case of an airfoil of span b and with elliptical loading). Here, the singular vortex sheet was first regularized in order to produce a vorticity field,

$$\omega_a(\mathbf{x}) = \frac{1}{\pi a^2}\int_{-b/2}^{b/2} \exp\left(-\frac{|\mathbf{x}-y\mathbf{e}_y|^2}{a^2}\right)\gamma(y)\,\mathrm{d}y \tag{13}$$

We here used $a/b = 2.5\times 10^{-3}$, thus still a very thin vortex sheet. The vorticity field was then discretized using particles put on multiple layers across the sheet, leading to a total of about 16 000 particles. The vortex method with Gaussian regularization function was used (using $\sigma = h$), with the fast multipole method (see below) and with particle redistribution (see later) done every 10 time steps. At the end of the simulation ($\tau \triangleq t/t_0 \approx 0.2$ where $t_0 \triangleq 2\pi b_0^2/\Gamma_0$), we had about 10^5 particles. It is seen that the method is able to capture fine structure dynamics: here Kelvin–Helmholtz instabilities developing on the vortex sheet as it rolls up.

3. 3-D vortex methods

The 3-D methods are presented: the *method of regularized vortex filaments* and the *method of regularized vortex particles*.

3.1. Vortex filaments

In 3-D inviscid flows, vortex lines move as material lines: this constitutes the basis for the *method of vortex filaments*. Each filament p corresponds to a vortex tube of circulation Γ_p: the strength associated to that filament. The method must be regularized as singular filaments have a logarithmically infinite self-induced velocity everywhere their curvature is nonzero. For filaments using radially symmetric regularization functions, one has

$$\mathbf{u}_\sigma(\mathbf{x}) = -\frac{1}{4\pi}\sum_p \Gamma_p \int_{C_p} \frac{g_\sigma(|\mathbf{x}-\mathbf{x}_p|)}{|\mathbf{x}-\mathbf{x}|^3}(\mathbf{x}-\mathbf{x}_p)\times \mathrm{d}\mathbf{x}_p \tag{14}$$

where the regularization function $g_\sigma(r) \triangleq g(\frac{r}{\sigma})$ is such that $g(\rho)\to 1$ for ρ large and $g(\rho)\propto\rho^3$ for ρ small. The corresponding streamfunction is obtained as

$$\boldsymbol{\psi}_\sigma(\mathbf{x}) = \frac{1}{4\pi}\sum_p \Gamma_p \int_{C_p} G_\sigma\big(|\mathbf{x}-\mathbf{x}_p|\big)\,\mathrm{d}\mathbf{x}_p \tag{15}$$

with $G_\sigma(r) \triangleq \frac{1}{\sigma}G(\frac{r}{\sigma})$ and $\frac{g(\rho)}{\rho^3} = -\frac{1}{\rho}\frac{\mathrm{d}G}{\mathrm{d}\rho}(\rho)$. This streamfunction also corresponds to the solution of $\nabla^2\psi_\sigma = -\omega_\sigma$ with

$$\boldsymbol{\omega}_\sigma(\mathbf{x}) = \sum_p \Gamma_p \int_{C_p} \zeta_\sigma\big(|\mathbf{x}-\mathbf{x}_p|\big)\,\mathrm{d}\mathbf{x}_p \tag{16}$$

where $\zeta_\sigma(|\mathbf{x}|) \triangleq \frac{1}{4\pi\sigma^3}\zeta(\frac{r}{\sigma})$ and $-4\zeta(\rho) = \frac{1}{\rho^2}\frac{\mathrm{d}}{\mathrm{d}\rho}(\rho^2\frac{\mathrm{d}G}{\mathrm{d}\rho}(\rho))$. One also obtains $\zeta(\rho) = \frac{1}{\rho^2}\frac{\mathrm{d}g}{\mathrm{d}\rho}(\rho)$ and thus $g(\rho) = \int_0^\rho \zeta(s)s^2\,\mathrm{d}s$. The normalization, $\int\zeta_\sigma(|\mathbf{x}|)\,\mathrm{d}\mathbf{x} = 1$, leads to $\int_0^\infty \zeta(\rho)\rho^2\,\mathrm{d}\rho = 1$. The vorticity and streamfunction, $\boldsymbol{\omega}_\sigma$ and $\boldsymbol{\psi}_\sigma$, are divergence free because the filaments are closed (or periodic); the velocity $\mathbf{u}_\sigma$ is divergence free because it is the curl of $\boldsymbol{\psi}_\sigma$. The method then consists in convecting all points on all filaments with their local velocity: $\frac{\partial}{\partial t}\mathbf{x}_p(\xi) = \mathbf{u}_\sigma(\mathbf{x}_p(\xi))$. It conserves the total vorticity $\boldsymbol{\Omega} = 0$, the impulse $\mathbf{I}$ and the angular impulse $\mathbf{A}$:

$$\mathbf{I} = \frac{1}{2}\sum_p \Gamma_p \int_{C_p} \mathbf{x}_p\times\mathrm{d}\mathbf{x}_p, \qquad \mathbf{A} = \frac{1}{3}\sum_p \Gamma_p \int_{C_p} \mathbf{x}_p\times(\mathbf{x}_p\times\mathrm{d}\mathbf{x}_p) \tag{17}$$

It also conserves the energy,

$$E = \frac{1}{4\pi}\sum_{p,q}\Gamma_p\Gamma_q \int_{C_p}\int_{C_q} G\big(|\mathbf{x}_p-\mathbf{x}_p|\big)\,\mathrm{d}\mathbf{x}_p\cdot\mathrm{d}\mathbf{x}_q \tag{18}$$

One typically uses parametric splines to numerically represent the filaments. The regularized method converges for regular vorticity fields when the number of filaments is increased, provided that the overlapping condition is satisfied. The regularization function has normalization $\int\zeta_\sigma(\mathbf{x})\,\mathrm{d}\mathbf{x} = 1$. It is of order r when it satisfies the moment properties $\int x_1^{p_1}x_2^{p_2}x_3^{p_3}\zeta_\sigma(\mathbf{x})\,\mathrm{d}\mathbf{x} = 0$ for $1\leqslant p_1+p_2+p_3 < r$, and $\int|\mathbf{x}|^r|\zeta_\sigma(\mathbf{x})|\,\mathrm{d}\mathbf{x} < \infty$. For radially symmetric functions, these become $\int_0^\infty\zeta(\rho)\rho^{2+s}\,\mathrm{d}\rho = 0$ for s even and $2\leqslant s < r$, and $\int_0^\infty|\zeta(\rho)|\rho^{2+r}\,\mathrm{d}\rho < \infty$. Order higher than $r=2$ calls for functions that are not strictly positive. See, e.g., [4] for a review list of typical functions and Table 2 for usual ones. The *low order algebraic* function has $r=0$: it can only be used for global vortex tube modelling (as done in the examples below), as it does not converge for detailed field discretizations (using many filaments per vortex tube). For detailed studies, we typically use filaments with $r=2$ functions: the *high order algebraic* function or the *Gaussian* function. The vortex filament method can also be used with σ different for each filament, provided that the method be symmetrized by replacing σ^2 by $\sigma_{pq}^2 = \frac{1}{2}(\sigma_p^2+\sigma_q^2)$ [5]: this ensures the conservation of impulse, angular impulse and energy.

Different choices of g_σ regularization function can be scaled with respect to each other (by changing σ) so as to have the same *long wavelength dynamics*: one then considers the dispersion relation (self-induced rotational velocity Ω) of bending perturbations on a line vortex (Kelvin's lowest order mode) for long wavelength perturbations ($k\sigma$ small), see [6,7]. Kelvin's long wave dispersion relation, derived for the top-hat vortex of radius a, is:

$$\Omega = \pm\frac{\Gamma}{4\pi}k^2\left[\log\left(\frac{ka}{2}\right)+\left(\gamma-\frac{1}{2}\right)+\frac{1}{4}\right] \tag{19}$$

where $\gamma = 0.5772\ldots$ is the Euler constant. With the vortex filament method, one obtains

$$\Omega = \pm\frac{\Gamma}{4\pi}k^2\left[\log\left(\frac{k\sigma}{2}\right)+\left(\gamma-\frac{1}{2}\right)+C\right] \tag{20}$$

Table 2
Examples of 3-D regularization functions

Function	$g(\rho)$	$G(\rho)$	$\zeta(\rho)$	r
Low order algebraic	$\frac{\rho^3}{(\rho^2+1)^{3/2}}$	$\frac{1}{(\rho^2+1)^{1/2}}$	$\frac{3}{(\rho^2+1)^{5/2}}$	0
High order algebraic	$\frac{\rho^3(\rho^2+5/2)}{(\rho^2+1)^{5/2}}$	$\frac{(\rho^2+3/2)}{(\rho^2+1)^{3/2}}$	$\frac{15/2}{(\rho^2+1)^{7/2}}$	2
Gaussian	$\mathrm{erf}(\frac{\rho}{2^{1/2}}) - \rho(\frac{2}{\pi})^{1/2}\mathrm{e}^{-\rho^2/2}$	$\frac{1}{\rho}\mathrm{erf}(\frac{\rho}{2^{1/2}})$	$(\frac{2}{\pi})^{1/2}\mathrm{e}^{-\rho^2/2}$	2

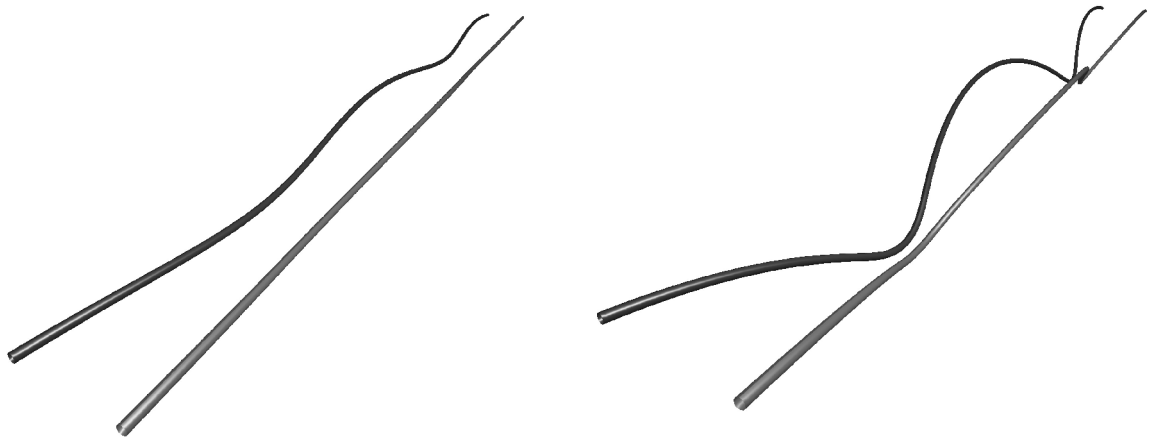

Fig. 2. Crow instability in a two-vortex system computed using the vortex filament method. Times shown are $\tau = 22.4$ and 23.7 (just before viscous reconnection would occur).

with $C = 1$ for the low order algebraic function, $C = 1/2$ for the high order algebraic function, and $C = 1.058$ for the Gaussian function: this provides the necessary relative scalings of σ to have the same dynamics.

An example of application of the method is shown in Fig. 2, for the case of a two-vortex system undergoing the Crow instability. The problem is periodic in x and a periodic version of the filament method is used. The period is $L_x/b_0 = 17.1$ (twice the theoretical most unstable wavelength). As the instability only involves bending of the vortex tubes, each vortex tube can be represented by one vortex filament; here a low order algebraic distribution, $\omega(r) = \frac{\Gamma}{2\pi}\frac{2\sigma^2}{(r^2+\sigma^2)^2}$ with $\sigma/b_0 = 0.091$; thus we use filaments with $\frac{g_\sigma(r)}{r^3} = \frac{r^2}{(r^2+\sigma^2)^{3/2}}$. We use parametric cubic splines ($x(i)$, $y(i)$ and $z(i)$) with 640 points per filament: the point to point spacing is thus $h/b_0 = 2.66 \times 10^{-2}$ (i.e., $h/\sigma = 0.294$). The filaments were initially perturbed using random displacement (maximum amplitude of $\varepsilon/b_0 \approx 1 \times 10^{-8}$). As usual, the times shown are expressed using $\tau \triangleq t/t_0$ with $t_0 = \frac{b_0}{V_0}$ where $V_0 = \frac{\Gamma_0}{2\pi b_0}$ is the vortex system descent velocity. The growth rate of the unstable Crow mode, evaluated from Fig. 3, is $\sigma_C t_0 \approx 0.77$.

Notice that the filament method was here also 'filtered'. Indeed, as $k\sigma$ is increased, the dispersion relation of filaments fails to follow Kelvin's lowest order bending mode (where Ω monotonically increases as $k\sigma$ increases), see [6,7]: it goes back down and eventually crosses the axis, thus leading to a non-rotating bending mode ($\Omega = 0$) when $k\sigma$ is of order unity (for the low-order algebraic, $k\sigma \approx 1.12$). If nothing is done, this spurious mode will pollute the simulation (and eventually make it blow up): filtering is necessary. Here, we used a discrete filter acting on the splines representation of the filaments. Defining the basic stencil-3 operator $\mathcal{P}$ acting on f_i (here $x(i)$, $y(i)$ and $z(i)$),

$$\mathcal{P} * f_i \triangleq -\frac{1}{4}[f_{i+1} - 2f_i + f_{i-1}] \tag{21}$$

and iterating it m times,

$$\mathcal{P}^m * f_i \triangleq \underbrace{\mathcal{P} * \mathcal{P} * \cdots * \mathcal{P}}_{m \text{ times}} * f_i \tag{22}$$

the filtered function $\overline{f}_i^{(m)}$ (filter of order m) is

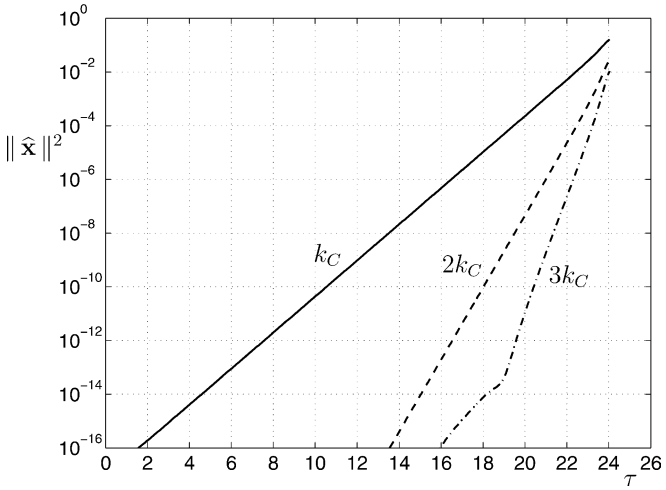

Fig. 3. Evolution of the modal displacement amplitude $\|\hat{\mathbf{x}}\|^2$ in a two-vortex system, for modes $kb_0 = 0.737$, 1.473, and 2.210 which correspond to the Crow mode (k_C) and its first two harmonics respectively.

$$\overline{f}_i^{(m)} \triangleq \mathcal{F}_m * f_i = f_i - \mathcal{P}^m * f_i \tag{23}$$

In Fourier space, the transfer function of this filter is $[1 - (\sin^2(\frac{kh}{2}))^m]$. If we apply the filtering n times,

$$\mathcal{F}_m^n * f_i = \underbrace{\mathcal{F}_m * \mathcal{F}_m * \cdots * \mathcal{F}_m}_{n \text{ times}} * f_i \tag{24}$$

this gives, as transfer function, $[1 - (\sin^2(\frac{kh}{2}))^m]^n$. We here used $m = 32$ and $n = 2$, and applied every two times steps: the damping then starts for modes at $kh/\pi \approx 0.1$ (thus here $kb_0 \approx 12$); those with $kh/\pi > 0.4$ (thus here $kb_0 > 47$) are essentially completely damped.

Another example is shown in Fig. 4 for the case of medium wavelength instabilities in a counter-rotating four-vortex system. This case, although a bit academic (as not easily achievable on a real aircraft), offers the possibility of fast growing instabilities (the so-called 'Omega' loops) as shown in [8–10], and thus provides potential for rapid changes in flow topology and the generation of small scale structures and turbulence through the strong interaction between unequal-strength opposite sign vortices (see also later for LES simulations done using the VIC method). Initially, we have $\Gamma_2/\Gamma_1 = -0.3$, $b_2/b_1 = 0.3$ (spacing ratio), $\sigma_1/b_1 = 0.075$ and $\sigma_2/\sigma_1 = 2/3$. Each vortex has the low-order algebraic distribution. We also define the *equivalent two-vortex system* (same half-plane global circulation and same linear impulse) by $\Gamma_0 = \Gamma_1 + \Gamma_2$ and $b_0 = (\Gamma_1 b_1 + \Gamma_2 b_2)/\Gamma_0$. The simulation extent corresponds to one wavelength of the Crow instability for the equivalent two-vortex system ($L_x/b_0 = 8.53$). The filaments were initially perturbed using a small random displacement (maximum amplitude of $10^{-7} b_1$). The time evolution of the perturbation amplitude of the unstable modes is also shown in Fig. 5. It is seen that the medium wave instability also acts as an amplifier of the Crow instability (see also [8]).

Clearly, the method of vortex filaments constitutes a simple and useful investigation tool for global vortex tube dynamics. Yet, it is limited to essentially inviscid studies (core growth by diffusion can be captured by varying σ). It does not allow for the reconnection of vortex tubes: something that can only happen by strong viscous interactions. Ad hoc *methods of filament surgery* have also been developed by some authors to artificially reconnect filaments of opposite sign and same strength, or to remove problematic parts of filaments. We do not follow such approaches. Instead, we use the viscous version of the vortex particle method, as presented in the next sections.

3.2. Vortex particles

We now consider the 3-D method of regularized vortex particles. One then associates to each vortical fluid element a volume V_p and a vector *strength* $\boldsymbol{\alpha}_p$, which is the integral of $\boldsymbol{\omega}$ over the material volume: $\boldsymbol{\alpha}_p = \int_{V_p} \boldsymbol{\omega}\, \mathrm{d}V \triangleq \boldsymbol{\omega}_p V_p$. The inviscid version

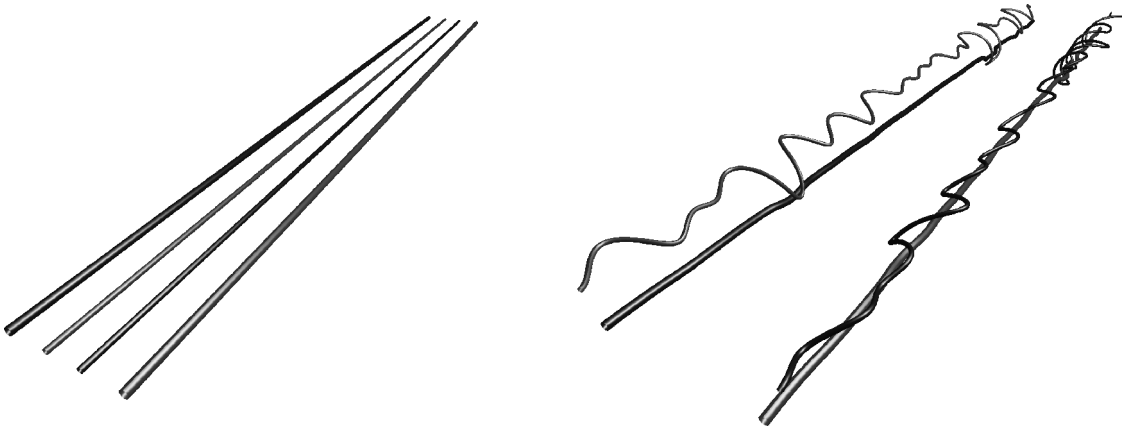

Fig. 4. Example of medium wavelength instabilities in a four-vortex system computed using the vortex filament method. Times shown are $\tau = 0$ and 0.88.

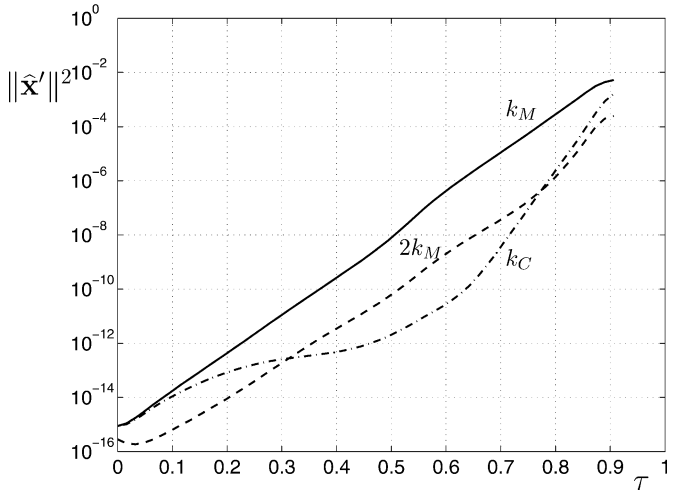

Fig. 5. Evolution of the modal perturbation amplitude $\|\hat{\mathbf{x}'}\|^2$ in a four-vortex system, for $k_M b_1 = 5.09$, $2k_M$ and $k_C b_1 = 0.567$ (Crow); $\sigma_M t_0 = 16.4$ (in $0.07 \leqslant \tau \leqslant 0.49$).

of the method can be written:

$$\frac{\mathrm{d}}{\mathrm{d}t}\mathbf{x}_p = \mathbf{u}_p, \qquad \frac{\mathrm{d}}{\mathrm{d}t}\boldsymbol{\alpha}_p = (\nabla \mathbf{u})_p \cdot \boldsymbol{\alpha}_p \tag{25}$$

The viscous version amounts to adding the diffusion term in the evolution equation for $\boldsymbol{\alpha}_p$ (see later). The methods converge as the number of particles is increased, provided the core overlapping condition is satisfied and that particle redistribution is done. It then allows for accurate long-time simulations of flows with regular vorticity field. Assuming

$$\tilde{\boldsymbol{\omega}}_\sigma(\mathbf{x}) = \sum_p \zeta_\sigma\big(|\mathbf{x} - \mathbf{x}_p|\big)\boldsymbol{\alpha}_p \tag{26}$$

one obtains

$$\tilde{\boldsymbol{\psi}}_\sigma(\mathbf{x}) = \frac{1}{4\pi}\sum_p G_\sigma\big(|\mathbf{x} - \mathbf{x}_p|\big)\boldsymbol{\alpha}_p, \qquad \mathbf{u}_\sigma(\mathbf{x}) = -\frac{1}{4\pi}\sum_p \frac{g_\sigma(|\mathbf{x} - \mathbf{x}_p|)}{|\mathbf{x} - \mathbf{x}_p|^3}(\mathbf{x} - \mathbf{x}_p) \times \boldsymbol{\alpha}_p \tag{27}$$

The method suffers from the fact that $\tilde{\boldsymbol{\omega}}_\sigma$ is not exactly equal to $\nabla \times \mathbf{u}_\sigma$, and thus that the particle fields, $\tilde{\boldsymbol{\omega}}_\sigma$ and $\tilde{\boldsymbol{\psi}}_\sigma$ are not generally divergence free. It appears, from experience in simulations, that the method is naturally well-behaved, at least when the simulation is well-resolved and when particle redistribution is used. Yet, for simulations covering a long time, and/or in under-resolved simulations, one eventually needs to re-enforce that the particle field remains a good representation of

$\boldsymbol{\omega}_\sigma = \nabla \times \mathbf{u}_\sigma$: *relaxation schemes* are thus required. The simplest relaxation scheme consists in resetting the particle strengths to the field: $\boldsymbol{\alpha}_p^{\text{new}} = \boldsymbol{\omega}_\sigma(\mathbf{x}_p)h^3$. This procedure is easy but quite diffusive.

In the VIC method (see later), an efficient and non-diffusive projection scheme is used instead. It is as follows: one first evaluates the discrete vorticity divergence on the grid, using finite differences acting on the redistributed particle weights: $\nabla_h \cdot \boldsymbol{\alpha}$; one then solves a Poisson equation on the grid: $\nabla_h^2 F = \nabla_h \cdot \boldsymbol{\alpha}$; the particles are then reset using: $\boldsymbol{\alpha}^{\text{new}} = \boldsymbol{\alpha} - \nabla_h F$, which ensures that the particle field is divergence free.

4. Viscous diffusion and LES

We already mentioned the viscous schemes to be used with particle method: for DNS, for LES, and even for RANS. We here present the scheme known as the *particle strength exchange* (PSE), see [11–13]. We develop it in 3-D; the 2-D case is obtained following the same procedure. In 3-D, one considers kernels such that $\int x_1^{p_1} x_2^{p_2} x_3^{p_3} \eta_\sigma(\mathbf{x})\,\mathrm{d}\mathbf{x} = 0$ for $1 \leqslant p_1 + p_2 + p_3 < 2 + r$, except that $\int x_i x_j \eta_\sigma(\mathbf{x})\,\mathrm{d}\mathbf{x} = \delta_{ij}\sigma^2$ (and thus $\int |\mathbf{x}|^2 \eta_\sigma(\mathbf{x})\,\mathrm{d}\mathbf{x} = 3\sigma^2$), and with $\int |\mathbf{x}|^{2+r} |\eta_\sigma(\mathbf{x})|\,\mathrm{d}\mathbf{x} < \infty$. In the case of radially symmetric kernels, $\eta_\sigma(|\mathbf{x}|) \stackrel{\triangle}{=} \frac{1}{4\pi\sigma^3}\eta(\frac{|\mathbf{x}|}{\sigma})$, the condition are $\int_0^\infty \eta(\rho)\rho^{4+s}\,\mathrm{d}\rho = 0$ for s even and $2 \leqslant s < r$, $\int_0^\infty \eta(\rho)\rho^4\,\mathrm{d}\rho = 3$, and $\int_0^\infty |\eta(\rho)|\rho^{4+r}\,\mathrm{d}\rho < \infty$. The following integral operator

$$(\nabla^2 f)_\sigma(\mathbf{x}) \approx \frac{2}{\sigma^2}\int \big(f(\mathbf{x}') - f(\mathbf{x})\big)\eta_\sigma(\mathbf{x}' - \mathbf{x})\,\mathrm{d}\mathbf{x}' \tag{28}$$

then provides an order σ^r approximation of the Laplacian. One can obtain order r kernels by using $\eta_\sigma(\mathbf{x}) = -\frac{\mathbf{x}\cdot(\nabla\zeta_\sigma(\mathbf{x}))}{(|\mathbf{x}|^2/\sigma^2)}$, with ζ an order r regularization (strictly positive kernels corresponding to $r = 2$). In the case of radially symmetric kernels, this gives $\eta(\rho) = -\frac{1}{\rho}\frac{\mathrm{d}\zeta}{\mathrm{d}\rho}(\rho)$ (as $\int_0^\infty \zeta(\rho)\rho^2\,\mathrm{d}\rho = 1$ indeed implies that $\int_0^\infty \eta(\rho)\rho^4\,\mathrm{d}\rho = 3$). In the particular case of the Gaussian, $\zeta(\rho) = (\frac{2}{\pi})^{1/2}\exp(-\rho^2/2)$, one obtains that $\eta(\rho) = \zeta(\rho)$.

To evaluate the integral operator, one simply performs a quadrature using the particles:

$$\begin{aligned}
\nu(\nabla^2 f)_\sigma(\mathbf{x}_p) &= \frac{2\nu}{\sigma^2}\sum_{q\in\mathcal{P}_p}(f_q - f_p)\eta_\sigma\big(|\mathbf{x}_q - \mathbf{x}_p|\big)V_q \\
\left(\frac{\mathrm{d}}{\mathrm{d}t}\alpha_p\right)_\nu &= \frac{2\nu}{\sigma^2}\sum_{q\in\mathcal{P}_p}(\alpha_q V_p - \alpha_p V_q)\eta_\sigma\big(|\mathbf{x}_q - \mathbf{x}_p|\big)
\end{aligned} \tag{29}$$

with $\alpha_p \stackrel{\triangle}{=} f_p V_p$ the particle strengths and $\mathcal{P}_p$ the ensemble of particles close enough to p that the interaction kernel is significant. Diffusion is thus done by particle strength exchange amongst neighbor particles. The scheme is conservative (as it should): $\sum_p \alpha_p$ is conserved. It can also be developed for non-uniform diffusion, as required in LES and RANS. One finally has, for the 3-D vortex method,

$$\frac{\mathrm{d}}{\mathrm{d}t}\boldsymbol{\alpha}_p = (\nabla\mathbf{u})_p \cdot \boldsymbol{\alpha}_p + \frac{1}{\sigma^2}\sum_{q\in\mathcal{P}_p}\big(\nu(\mathbf{x}_q) + \nu(\mathbf{x}_p)\big)(\boldsymbol{\alpha}_q V_p - \boldsymbol{\alpha}_p V_q)\eta_\sigma\big(|\mathbf{x}_q - \mathbf{x}_p|\big) \tag{30}$$

and, for the 2-D vortex method,

$$\frac{\mathrm{d}}{\mathrm{d}t}\Gamma_p = \frac{1}{\sigma^2}\sum_{q\in\mathcal{P}_p}\big(\nu(\mathbf{x}_q) + \nu(\mathbf{x}_p)\big)(\Gamma_q S_p - \Gamma_p S_q)\eta_\sigma\big(|\mathbf{x}_q - \mathbf{x}_p|\big) \tag{31}$$

The 2-D and 3-D viscous methods also require that the particles remain fairly uniformly spaced as the simulation proceeds, and thus also particle redistribution. Regions of low vorticity also need to be able to diffuse towards regions of even lower vorticity. Hence, particles must be present where needed; this is also a task performed by the redistribution step.

The viscous vortex particle methods can be used to solve any convection-diffusion equations (eventually also with source terms, as for RANS). In the case of LES, a subgrid-scale (sgs) model is used to dissipate energy at the smallest resolved scales. For instance, one can use an effective viscosity sgs model (e.g., the Smagorinsky model). Such model can also be combined with a hyper-viscosity model (easily obtained by applying recursively the PSE scheme) so as to form a mixed model.

There is also the modeling procedure proposed by [14] (see also [1,2]) and originally developed to compensate for truncation errors in 2-D vortex methods: it amounts to further correcting the particle strengths using a PSE-like version of the so-called *tensor-diffusivity model* (TDM):

$$\frac{\mathrm{d}}{\mathrm{d}t}\Gamma_p = \frac{1}{\sigma^2}\sum_{q\in\mathcal{P}_p}\big[2\nu + \big(\mathbf{u}_\sigma(\mathbf{x}_q) - \mathbf{u}_\sigma(\mathbf{x}_p)\big)\cdot(\mathbf{x}_q - \mathbf{x}_p)\big](\Gamma_q S_p - \Gamma_p S_q)\eta_\sigma\big(|\mathbf{x}_q - \mathbf{x}_p|\big) \tag{32}$$

To avoid problems related to negative diffusion effects, clipping is also used: by retaining only the interactions with $[2\nu + (\mathbf{u}_\sigma(\mathbf{x}_q) - \mathbf{u}_\sigma(\mathbf{x}_p))) \cdot (\mathbf{x}_q - \mathbf{x}_p)] \geqslant 0$. This scheme significantly improves the behavior of the vortex method at the fine scales. It can also be used as sgs model for LES: one then puts a C constant in front of the clipped TDM part: use $[2\nu + C(\mathbf{u}_\sigma(\mathbf{x}_q) - \mathbf{u}_\sigma(\mathbf{x}_p)) \cdot (\mathbf{x}_q - \mathbf{x}_p)]$.

As to *quasi-inviscid simulations* (*quasi-Euler*), we here mean simulations without viscosity and without sgs viscosity-type model. Such simulations are used to model flows in the limit of very high Reynolds number. In 3-D, some sgs hyper-viscosity term is nevertheless required, as the small dissipation produced by the particle redistribution operation is not sufficient.

As an illustration of the 2-D viscous vortex particle method, we present an example of roll-up of a near wake, starting from wind tunnel experimental data (five-hole probe and PIV data) on a generic configuration consisting of a fuselage and a flapped wing (the *SWIM* configuration, see [15]). The comparison between experimental measurements and simulations are presented in Figs. 6, 7 and 8. We first used diffusion based on a uniform *effective turbulence viscosity*, ν_t (thus a very simplified RANS approach) set according to the scaling proposed by Owen [16] (see also [17]):

$$\frac{\nu_t}{\nu} = \frac{1}{\beta}\sqrt{\frac{\Gamma_0}{\nu}} \quad \Longleftrightarrow \quad \frac{\Gamma_0}{\nu_t} = \beta\sqrt{\frac{\Gamma_0}{\nu}} \quad \Longleftrightarrow \quad Re_t = \beta\sqrt{Re} \tag{33}$$

The factor β was set to 8 as calibrated on one SWIM data set, on the criterion that the time of merging of the co-rotating vortices be comparable to that in the experiments; it was then showed to be appropriate for the other SWIM data sets, and even for data sets related to other projects and at higher Reynolds numbers (not shown). With the SWIM data set, this led to using $Re_t = 4 \times 10^3$. The vortex method was run at high resolution, (using $h = b/400$ with b the wingspan), using the Gaussian regularization function (with $\sigma = h$), and with particle redistribution done every 10 time steps. One globally observes a good agreement for the evolution of the roll-up process; even the details of the filamentation can be compared.

It is important to stress that the merging process is here a *stable* merging: as opposed to the *unstable* case corresponding to the merging of vortices that are further apart, and that can happens through 3-D short wave instabilities, their saturation and the turbulence they generate. The case of stable merging can indeed satisfactorily be captured using 2-D RANS. The case of 3-D unstable merging calls for using 3-D LES (see later). Of course, RANS with the assumption of uniform turbulence viscosity constitutes an oversimplification: one captures properly much of the physics and the global features, but the vortex cores are too diffused. RANS models that take into account the spatial variability are eventually needed;

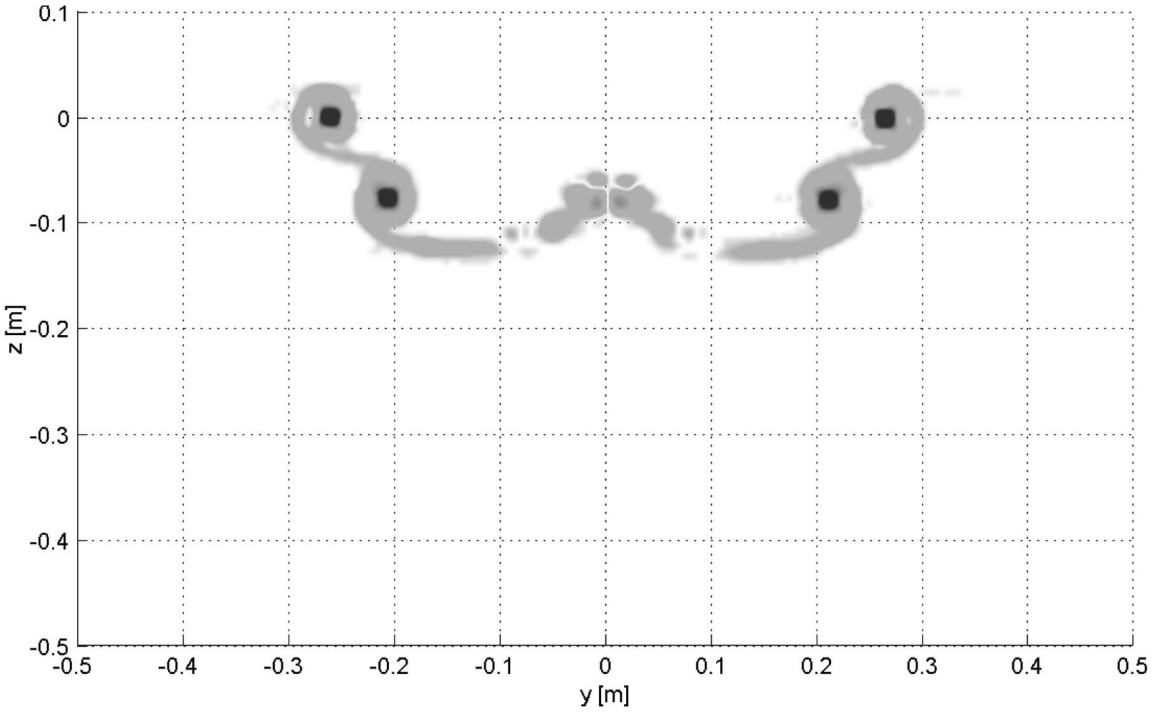

Fig. 6. Initial vorticity field at $x/b = 1.25$ for configuration 1, from experimental measurement (SWIM, five-holes probes) cleaned up for simulation.

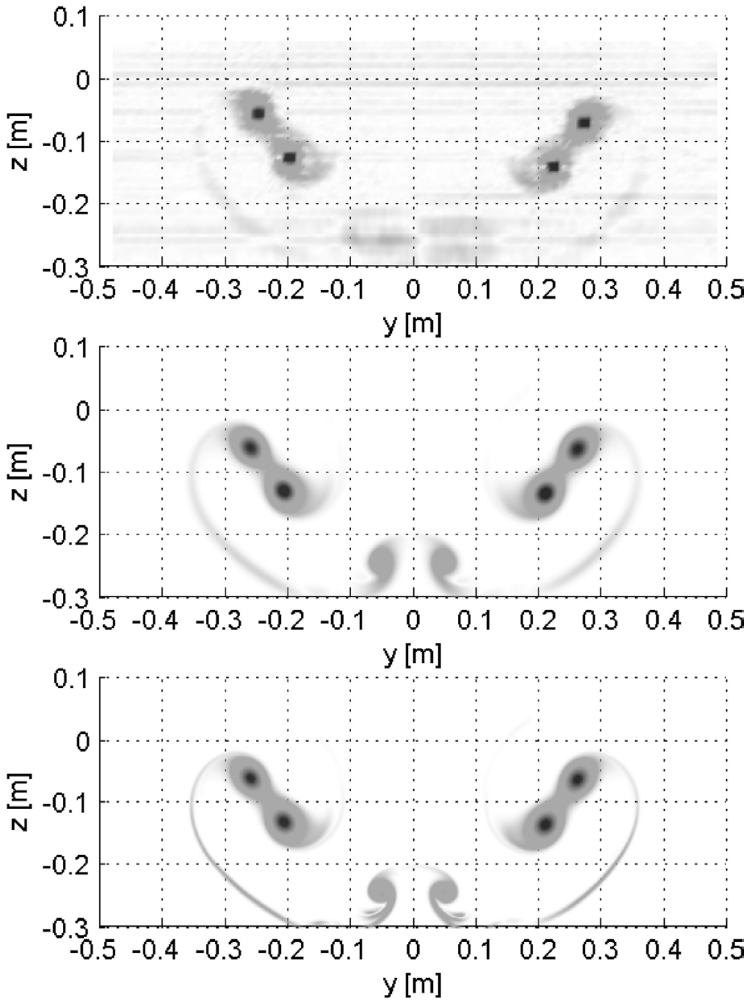

Fig. 7. Vorticity field at $x/b = 5$ for configuration 1. Top: obtained from five-hole probes velocity measurements; middle: simulation using a uniform effective viscosity; bottom: simulation using the clipped TDM.

those are also required to model the enhanced mixing across the centerline due to the turbulence created by the fuselage wake.

As another example, we also considered a simulation using instead the clipped TDM model and with $C = 2$ (also calibrated for obtaining the proper time of stable merging). This model performs quite well: it can be shown to produce negligible diffusion in regions with pure rotation (i.e., within the vortex core); yet it produces sufficient diffusion to capture the turbulent interactions between the vortices and thus the merging. The agreement with the experimental data is seen to be better than for the case with uniform effective viscosity. We also expect that the clipped TDM model will constitute an interesting sgs model for 3-D LES, because of the negligible diffusion in regions with pure rotation; this remains to be investigated.

5. Particle redistribution

Previously, we have often mentioned the need for *particle redistribution*. Without it, Lagrangian methods fast loose their accuracy as the simulation proceeds, because the condition of distribution uniformity, that is required for overlap of the particle regularization functions, does not remain satisfied. The commonly used redistribution schemes are presented (see also [1,2]): one makes use of a regular redistribution lattice of size h; the old set of particles is replaced by a new set, the new particles being on the lattice. First consider the 1-D problem. Denoting U the distance (normalized by h) between the old particle and a new

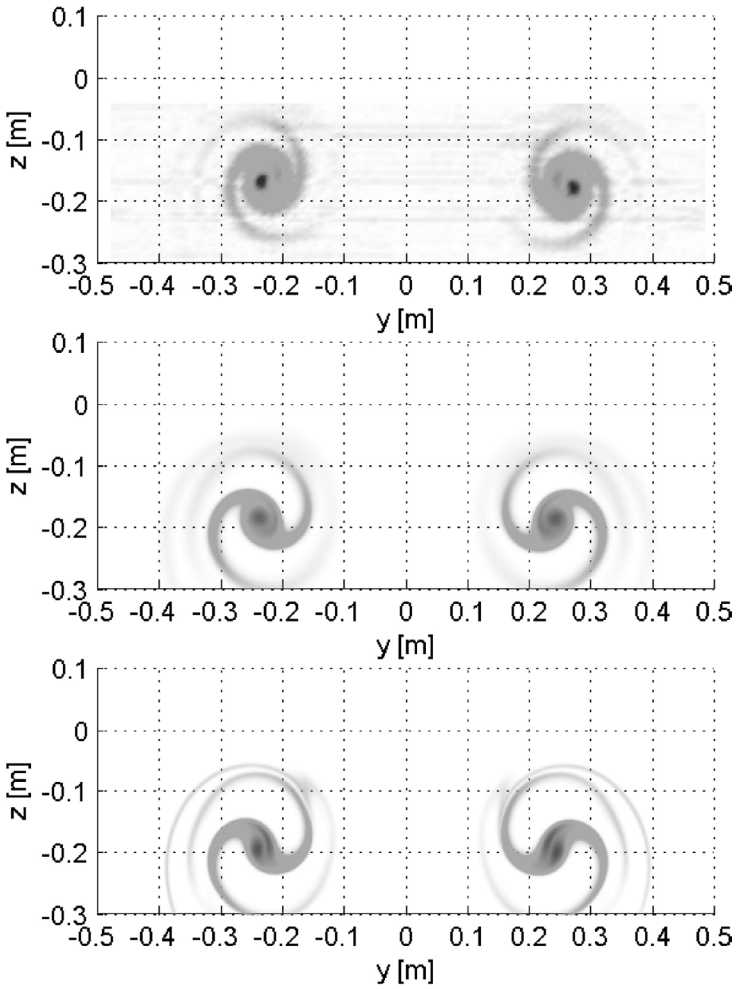

Fig. 8. Vorticity field at $x/b = 10.25$ for configuration 1. Top: obtained from five-hole probes velocity measurements; middle: simulation using a uniform effective viscosity; bottom: simulation using the clipped TDM.

one, the fraction of the old particle strength that is attributed to a new particle is denoted $\Lambda_r(U)$ (r meaning that it conserves the moments up to order r: from $\sum_p \alpha_p$ up to $\sum_p x_p^r \alpha_p$). The zero and second order schemes are:

$$\Lambda_0(U) = \begin{cases} 1 & \text{if } U < \frac{1}{2} \\ 0 & \text{otherwise} \end{cases} \qquad \Lambda_2(U) = \begin{cases} 1 - U^2 & \text{if } 0 \leqslant U < \frac{1}{2} \\ \frac{1}{2}(1-U)(2-U) & \text{if } \frac{1}{2} \leqslant U < \frac{3}{2} \\ 0 & \text{otherwise} \end{cases} \tag{34}$$

Both schemes are discontinuous: $\Lambda_0(U)$ at $\frac{1}{2}$; $\Lambda_2(U)$ at $\frac{1}{2}$ and $\frac{3}{2}$. The first and third order schemes are:

$$\Lambda_1(U) = \begin{cases} 1 - U & \text{if } 0 \leqslant U \leqslant 1 \\ 0 & \text{otherwise} \end{cases} \qquad \Lambda_3(U) = \begin{cases} \frac{1}{2}(1-U^2)(2-U) & \text{if } 0 \leqslant U \leqslant 1 \\ \frac{1}{6}(1-U)(2-U)(3-U) & \text{if } 1 \leqslant U \leqslant 2 \\ 0 & \text{otherwise} \end{cases} \tag{35}$$

Both schemes are continuous, which leads to better numerical results (less high frequency noise after redistribution). It is also worth mentioning another popular scheme: the M_4' scheme,

$$M_4'(U) = \begin{cases} 1 - \frac{5}{2}U^2 + \frac{3}{2}U^3 & \text{if } 0 \leqslant U \leqslant 1 \\ \frac{1}{2}(1-U)(2-U)^2 & \text{if } 1 \leqslant U \leqslant 2 \\ 0 & \text{otherwise} \end{cases} \tag{36}$$

It is continuous and so is its first derivative. It has width 4 and is of second order.

In multiple dimensions, the redistribution schemes are obtained using products of 1D schemes: $\Lambda_r(U,V) = \Lambda_r(U)\Lambda_r(V)$ in 2D, $\Lambda_r(U,V,W) = \Lambda_r(U)\Lambda_r(V)\Lambda_r(W)$ in 3D. The $\Lambda_1(U)$ scheme is what was commonly used in the first vortex-in-cell (VIC) methods; it should be avoided as it is quite dissipative. Nowadays, the $\Lambda_3(U)$ or the M_4' schemes are most often used, including for VIC; they are much less dissipative (hyper-viscosity behavior).

The redistribution lattice needs not be uniform; it can stretch, as long as the stretching rate remains moderate. This is most useful, as it allows to tailor the spatial resolution of simulations. The above redistributions schemes are then applied within the uniform index space (this does not conserve exactly the moments; yet, with moderate stretching rate, the behavior of the method is still acceptable, as redistribution is a local operator). The same goes for diffusion: the symmetrized PSE,

$$\frac{\mathrm{d}}{\mathrm{d}t}\alpha_p = 2\nu \sum_{q\in\mathcal{P}_p} \frac{1}{\sigma_{pq}^2}(\alpha_q V_p - \alpha_p V_q)\eta_{\sigma_{pq}}(\mathbf{x}_p - \mathbf{x}_q) \tag{37}$$

still yields a second order scheme, provided that the local σ variations are small (this is the case since particles are regularly redistributed on a lattice with moderate stretching, and their σ is set proportional to h of the local lattice), see [18].

6. Efficient velocity evaluation: fast multipole method and vortex-in-cell method

The Green's function (i.e., Biot and Savart) direct evaluation of the velocity (and, in 3-D, its gradient) induced by N vortex elements, at M locations requires $\mathcal{O}(MN)$ operations. This precludes large-scale simulations. Fast methods have been developed, both in 2-D and in 3-D, that have an operation count of $\mathcal{O}(M\log N)$ (or even $\mathcal{O}(N)$ depending on the details of the algorithm), see, e.g., [19–21]. The basic idea of these methods is to decompose the element population spatially into clusters of particles and build a hierarchy of clusters (*tree*: quad-tree in 2-D, oct-tree in 3-D)—smaller neighboring clusters combine to form a cluster of the next size up in the hierarchy and so on.

Each cluster is represented by its multipole expansion, expressed with respect to an expansion center, $\mathbf{x}_c$ (e.g., use the 'centroid': $\mathbf{x}_c = (\sum_p \mathbf{x}_p|\alpha_p|)/(\sum_p|\alpha_p|)$) [22]. In 3-D, this gives

$$\begin{aligned} 4\pi\boldsymbol{\psi}_\sigma(\mathbf{x}) &= \int G_\sigma\big(|\mathbf{x}-\mathbf{x}'|\big)\boldsymbol{\omega}(\mathbf{x}')\,\mathrm{d}\mathbf{x}' \\ &= G_\sigma\big(|\mathbf{x}-\mathbf{x}_c|\big)\mathbf{M}^{(0)} - \partial_i G_\sigma\big(|\mathbf{x}-\mathbf{x}_c|\big)\mathbf{M}_i^{(1)} + \frac{1}{2}\partial_i\partial_j G_\sigma\big(|\mathbf{x}-\mathbf{x}_c|\big)\mathbf{M}_{ij}^{(2)} - \cdots \end{aligned} \tag{38}$$

where $\mathbf{M}^{(0)} = \int \boldsymbol{\omega}(\mathbf{x}')\,\mathrm{d}\mathbf{x}'$, $\mathbf{M}_i^{(1)} = \int (\mathbf{x}'-\mathbf{x}_c)_i\boldsymbol{\omega}(\mathbf{x}')\,\mathrm{d}\mathbf{x}'$, $\mathbf{M}_{ij}^{(2)} = \int (\mathbf{x}'-\mathbf{x}_c)_i(\mathbf{x}'-\mathbf{x}_c)_j\boldsymbol{\omega}(\mathbf{x}')\,\mathrm{d}\mathbf{x}'$, etc. are the monopole, dipole, quadrupole moments of the distribution. With particles, one obtains $\mathbf{M}^{(0)} = \sum_p \boldsymbol{\alpha}_p$, $\mathbf{M}_i^{(1)} = \sum_p (\mathbf{x}_p-\mathbf{x}_c)_i\boldsymbol{\alpha}_p$, $\mathbf{M}_{ij}^{(2)} = \sum_p (\mathbf{x}_p-\mathbf{x}_c)_i\boldsymbol{\alpha}_p(\mathbf{x}_p-\mathbf{x}_c)_j$, etc, where the sum runs over the particles of the cluster. For the singular kernel, $G(r) = 1/r$, one obtains

$$4\pi\boldsymbol{\psi}(\mathbf{x}) = \frac{1}{|\mathbf{x}-\mathbf{x}_c|}\mathbf{M}^{(0)} + \frac{1}{|\mathbf{x}-\mathbf{x}_c|^2}e_i\mathbf{M}_i^{(1)} + \frac{1}{2}\frac{3}{|\mathbf{x}-\mathbf{x}_c|^3}\left(e_ie_j - \frac{1}{3}\delta_{ij}\right)\mathbf{M}_{ij}^{(2)} + \cdots \tag{39}$$

The expansion of any regular kernel (e.g., $G_\sigma(r) = 1/(r^2+\sigma^2)^{1/2}$ as used in [21], or any other one) is also easily obtained. The multipole expansion of a cluster can then be used to obtain the fields (streamfunction, velocity (by differentiating once the expansion), velocity derivatives (by differentiating twice)) at any point outside the smallest ball of radius b containing all the cluster particles and centered at $\mathbf{x}_c$. The absolute error, $e_{|\mathbf{u}|}$, made on the velocity evaluated at a distance $d > b$ can be bound tightly for multipole expansions of any function and of any order (see [21]). In 3-D, one typically uses expansions with $p = 2$ (monopole + dipole + quadrupole terms). The following *tight error bounds* are then obtained:

$$\begin{aligned} e_{|\boldsymbol{\psi}|} &\leqslant e_{|\boldsymbol{\psi}|}^{\text{bound}} = \frac{B_0}{4\pi(d-b)}\left(\frac{B_2}{B_0b^2}\right)\left(\frac{b}{d}\right)^3 \\ e_{|\mathbf{u}|} &\leqslant e_{|\mathbf{u}|}^{\text{bound}} = \frac{B_0}{4\pi(d-b)^2}\left[4\left(\frac{B_2}{B_0b^2}\right)\left(\frac{b}{d}\right)^3 - 3\left(\frac{B_2}{B_0b^2}\right)^2\left(\frac{b}{d}\right)^4\right] \end{aligned} \tag{40}$$

where $B_0 = \sum_p|\alpha_p|$ and $B_2 = \sum_p|\mathbf{x}_p-\mathbf{x}_c|^2|\alpha_p|$ are cluster properties. For each cluster, this equation determines d_{crit} corresponding to a prescribed tolerance, $e_{|\mathbf{u}|}^{\text{tol}}$: a cluster property. The multipole expansion of a cluster contributes to the velocity at an evaluation point if the distance d of the point to $\mathbf{x}_c$ is greater than d_{crit} (and, when using expansion of the singular kernel for problems with regularized particles, if the point is outside of the region influenced by the regularization: $d-b \geqslant n\sigma$ where

n depends on the regularization function). Otherwise, the cluster is not used and the test is applied recursively to all active *children* clusters within that cluster. If a smallest size cluster has been reached and the error criterion is still not satisfied, one then proceeds with direct evaluation of the velocity induced by the regularized particles in that smallest cluster. A good estimate of the final error for the velocity evaluated at one point is the square root of the sum of the error bounds squared for all multipoles used to compute the velocity at that point. In 3-D, one typically ends up with a mean actual error bound equal to three to five times the prescribed $e^{\mathrm{tol}}_{|\mathbf{u}|}$: a comforting result. Fast 3-D tree-codes have also been developed so as to run on massively parallel computers with distributed memory: the *parallel fast multipole method* (PFMM). Computations using many processors have been carried out, with a very good parallel performance, see, e.g., [21,22].

An efficient alternative to using fast multipole methods (FMM) is to use grid-based Poisson solvers. Efficient solvers (e.g., the Fishpack software) have an $\mathcal{O}(M \log M)$ computational cost (M being the number of grid points), and the constant in front is much smaller than that associated with the best $\mathcal{O}(N \log N)$ FMM. Such approach then calls for a hybrid particle-grid method: the so-called *vortex-in-cell method* (VIC). It was first introduced by [23], and then further used and developed by others (see [1] and references therein, and also [24,25,30,34]). At each time step, the VIC method uses projection of the particle strengths onto the grid, and the projection of the grid-solved velocity (and its gradient in 3-D) back onto the particles. These are easily achieved using the high redistributions schemes as interpolation schemes (e.g., M'_4).

Note that VIC still retains the main advantage of the vortex method: as the particles are still convected in a Lagrangian way, the method still has negligible dispersion error. Moreover, since there is a grid, the diffusion term (DNS, LES or RANS) can be evaluated using the grid (i.e., no need to use a PSE scheme). The grid-evaluated diffusion term is interpolated back to the particles using the same interpolation scheme as that used for the velocities.

Of course, as $\nabla^2 \boldsymbol{\psi} = -\boldsymbol{\omega}$ is solved on a grid, one must use a large domain so as to be able to provide approximate analytical boundary conditions on $\boldsymbol{\psi}$ on the sides of the computational grid. Alternatively, one could assume that the problem is periodic. In either cases, the approximation of an open-domain flow requires that the computational grid be quite large.

An efficient alternative has recently been developed within our group: use the VIC methodology, but with the exact boundary conditions obtained using the fast multipole method (FMM). This combination VIC-FMM is very efficient: a compact VIC grid, enclosing tightly the non-zero vorticity field can be used, while the boundary condition is still enforced exactly.

Furthermore, the method can also easily be parallelized, using the domain decomposition method: each processor handles its own subdomain (local solution of the Poisson equation using the grid-solver); the parallel fast multipole method (PFMM) code, which has a global view of the whole field, is used to obtain the exact boundary conditions on each subdomain. Notice that all is done without iteration between the subdomains: the VIC-PFMM combination amounts to an efficient parallelized Poisson solver (one without any iteration).

As example of application, the case of medium wavelength instabilities in a four-vortex system is again considered, see Fig. 9. The initial perturbation was done such that the centerlines of the vortices were displaced, perpendicular to the longitudinal x-axis, using a small-amplitude sine wave. In order to determine the wavelength of the most unstable mode, a parametric study was done using the vortex filament code: it was determined that $kb_1 = 6.39$ (or equivalently that $\lambda/b_1 = 0.983$) had the fastest growing behavior. The problem is periodic in x (with $L_x/b_1 = 0.983$) but not in y and z. The discretization is $h/L_x = 1/64$. A M'_4 redistribution is done every time step. It is a quasi-inviscid simulation, and we use a hyper-viscosity sgs model (obtained by iterating twice a grid-evaluated Laplacian):

$$\frac{D\boldsymbol{\omega}}{Dt} = (\nabla \mathbf{u}) \cdot \boldsymbol{\omega} - \frac{C}{t_0} \left(h^2 \nabla_h^2\right)^2 \boldsymbol{\omega} \tag{41}$$

with $C = 6.8$ (i.e., $Ch^4/t_0 = 2.5 \times 10^{-8}$). The simulation was run using the VIC-PFMM combination on 4 processors (an x-periodic version of the PFMM was used to obtain the boundary conditions on each VIC subdomain). The total VIC grid grew from $64 \times 127 \times 65$ to $64 \times 305 \times 178$ (3.5 millions), and the number of particles from 0.36 to 1.8 millions. The results are also usefully compared to those obtained using a reference spectral method (here with high order, k^8, hyperviscosity sgs model): it is seen, in Figs. 10 and 11, that the instabilities, their growth, and the non-linear interactions (including the energy decay) are very well captured by the present method. Note that a DNS case, at $Re = \Gamma_1/\nu = 5000$, was also performed: it is presented in [2].

To further illustrate the capability of the parallel method, a case where the simulation extends over one Crow wavelength of the equivalent two-vortex system was also done: $L_x/b_1 = 11.1$ (i.e., $L_x/b_0 = 8.53$). Here, a small level random initial perturbation (max magnitude $10^{-5} b_1$) was applied. The simulation ran 5800 time steps in 65 hours on 48 processors. The VIC grid grew from $720 \times 128 \times 64$ to $720 \times 310 \times 312$ (70 millions) and the number of vortex particles from 3.3 to 18 millions. The 3-D field energy evolution is shown in Fig. 12: again, this compares well with that obtained using the reference spectral method. The vorticity field is shown in Fig. 13: this too compares well with the spectral results. The VIC-PFMM combination is clearly able to accurately and efficiently simulate very complex and large scale flows.

Finally, a four-vortex system with co-rotating vortices is considered, see Fig. 14. This is a case with unstable merging of the co-rotating vortices, thus requiring 3-D LES. The parameters are $\Gamma_2/\Gamma_1 = 0.4$, $b_2/b_1 = 0.5$, $\sigma_1/b_1 = 0.05$, $\sigma_2/b_1 = 0.025$,

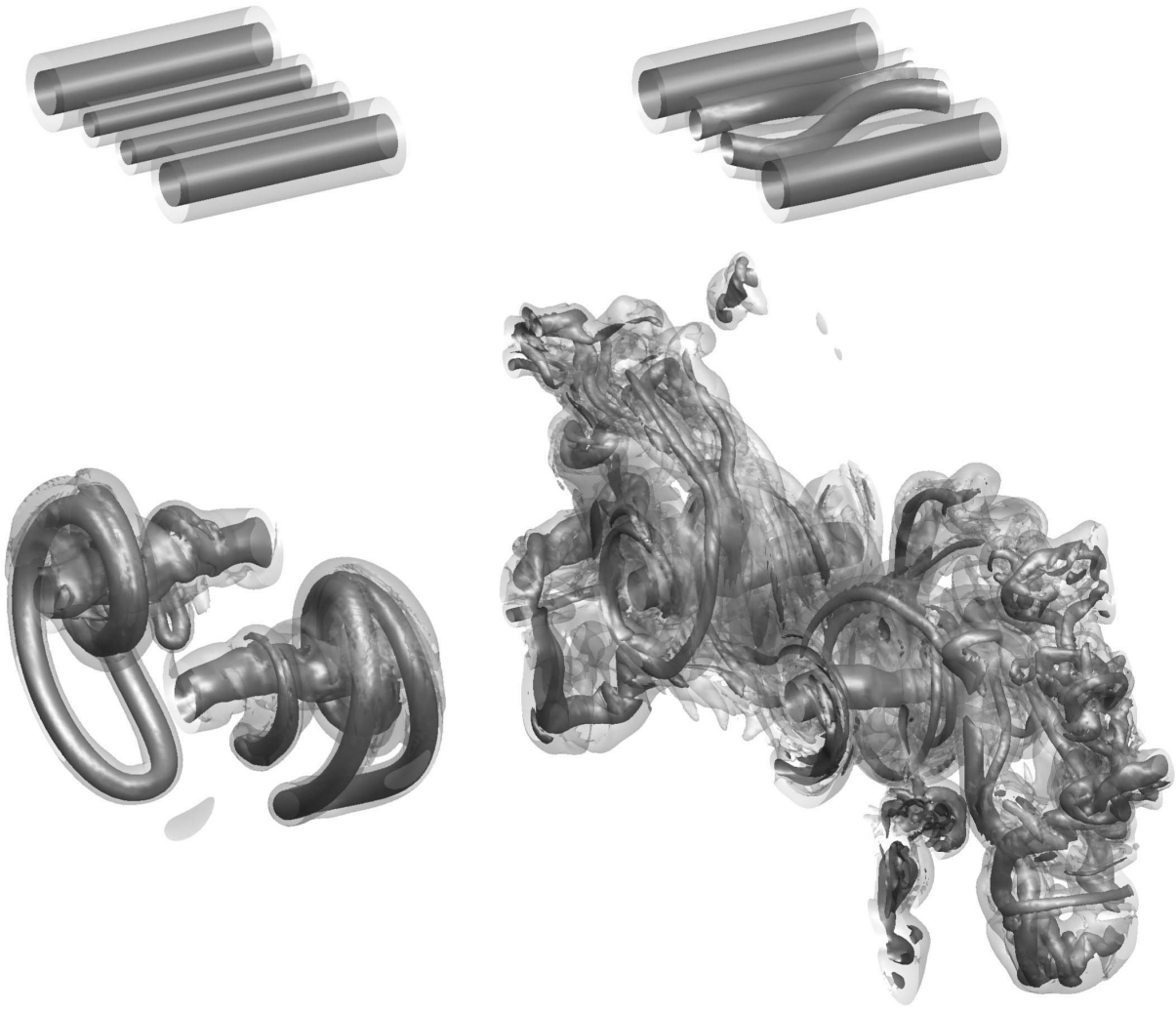

Fig. 9. Evolution of the four vortex system as obtained using the VIC-PFMM code. Iso-surfaces of vorticity modulus shown are $|\boldsymbol{\omega}|b_1^2/\Gamma_1 = 10.0$ (high opacity) and 2.0 (low opacity). Times are $\tau = 0.0$, 0.61, 0.79 and 1.05.

$L_x/b_1 = 1$, $h/L_x = 1/100$. It ran for 2500 time steps on 8 processors; the grid grew from $100 \times 173 \times 73$ to $100 \times 181 \times 181$ (3.3 million) and the number of particles from 0.75 to 1.1 million.

7. Cases with solid boundaries

Nowadays, vortex methods are also used efficiently to simulate unsteady flows with solid boundaries. One then needs to evaluate, at each time step, the vorticity flux emitted at each point on the solid surface, in order to satisfy the no-slip condition after the vorticity has been convected and diffused [26–28]. For general geometries, this flux is obtained as the solution of an integral equation, itself discretized using panels. The vortex method is thus combined with a *boundary element method* (BEM). This flux is emitted using a PSE-like scheme [27,28]; it ends up providing an update of the nearby vortex particles.

In the first step, one convects the particles with the local velocity and updates their strength according to the PSE (eventually modified near the boundary, so as to have a zero flux of tangential vorticity (and a zero normal vorticity in 3-D), as in [18,29]; this is however not fully necessary, see [30]). After this step, there is a spurious slip velocity, $\delta\mathbf{u}_{\text{slip}}$, seen at the boundary. The vortex sheet, $\delta\gamma$, necessary to cancel this slip velocity is then computed using BEM. The boundary is discretized using M boundary elements (i.e., *vortex sheet panels*), each of size $\mathrm{O}(h)$ (with h the typical distance between particles near the boundary) and each of unknown strength. For each panel on the body, the mean slip velocity underneath that panel is taken as the average, over the

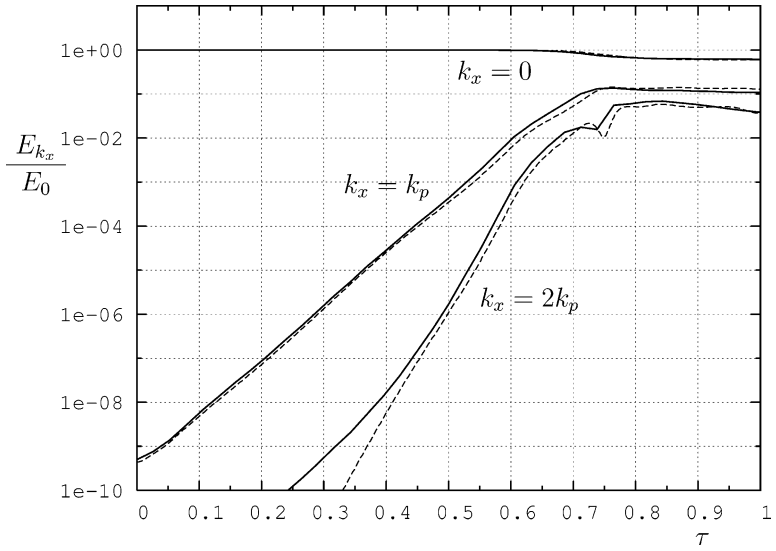

Fig. 10. Evolution of the modal energy E_{k_x} for the base flow mode $k_x = 0$, the perturbed mode $k_x = k_p$ and its first harmonic $k_x = 2k_p$: VIC-PFMM method (solid) and spectral method (dash). The modal energy is normalized using the initial unperturbed base-flow field energy E_0 .

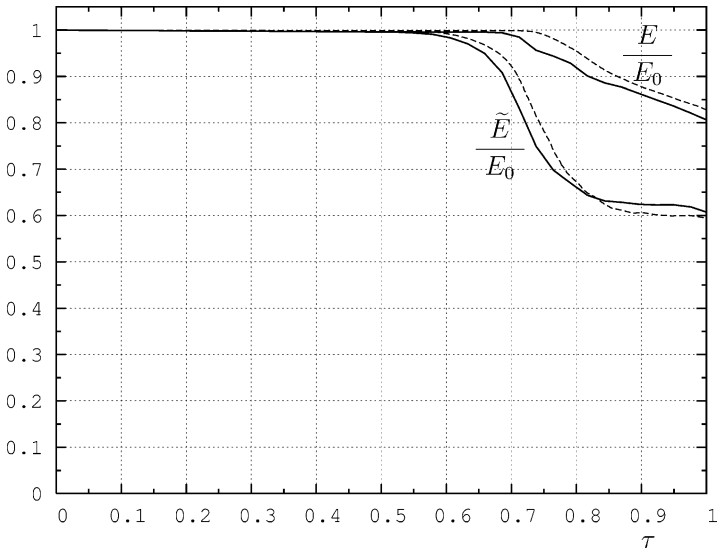

Fig. 11. Evolution of kinetic energy for the VIC-PFMM method (solid) and the spectral method (dash): energy of 3-D field, E, and energy of longitudinally-averaged (2-D) field, $\widetilde{E}$.

panel, of the velocity induced by the freestream and all vortex particles (considered as point vortices, to ensure that all vorticity is outside of the boundary), see [27,18,29,33]. Once the slip velocity has been evaluated for all panels, obtaining the panel strengths so as to cancel this slip velocity amounts to solving an integral equation: thus a linear system of the form $A\delta\gamma = b$ where A is full, since, in addition to inducing a tangential velocity underneath themselves (equal to $\frac{\delta\gamma}{2}$), the panels induce a velocity on one another). The velocity induced by all M panels on all M panels, which corresponds to the operation $A\delta\gamma$, is thus also an M-body problem: it can also be evaluated efficiently using the FMM. Thus, the system is solved using an iterative method, with FMM used at each iteration. Such fast BEM method allows for large numbers of panels (easily 10^4 to 10^5 in 3-D, as in [29]).

The total flux to be emitted into the flow, for the other substep of the diffusion process, is then given by $\nu\frac{\partial\omega}{\partial n} = \frac{\delta\gamma}{\delta t}$. This flux must be emitted during a time δt. In effect, the vortex sheet $\delta\gamma$ must be distributed to neighbor particles by discretizing the Green's integral for the inhomogeneous Neumann problem corresponding to the diffusion equation, [26,27,18,29,1,2]: the

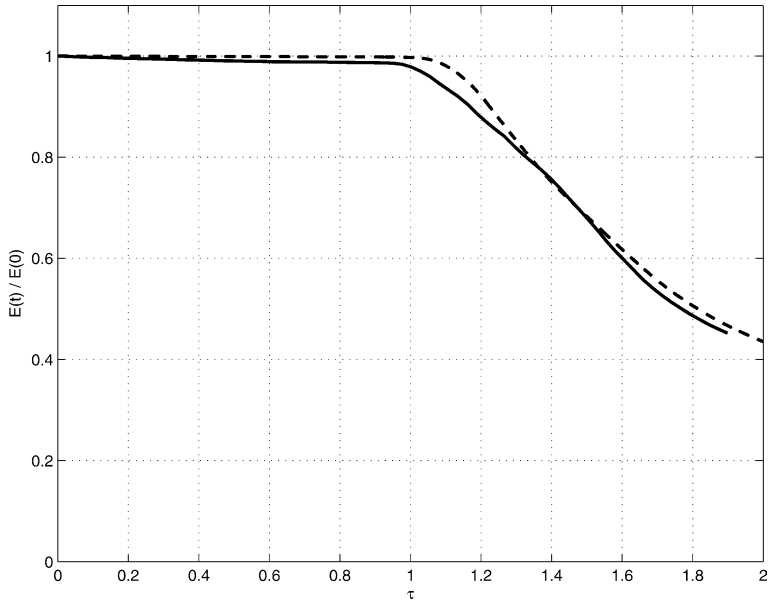

Fig. 12. Four vortex system over a long domain. Evolution of the kinetic energy: VIC-PFMM method (solid) and spectral method (dash).

obtained formulas amount to an update of the particles near the panel, so as to absorb this flux; at the end, $\delta\gamma$ is completely distributed to the nearby particles.

Instead of the pure fast multipole method, the VIC method with body fitted grid can also be used [31,25]. Yet another method is the combination of VIC and immersed boundaries techniques, see [25,30]: the VIC grid then crosses the body surface arbitrarily and the Poisson equation is solved everywhere (inside and outside); the vorticity flux is obtained by solving an integral equation for the required singularities, and discretized using the grid points nearest to the surface.

As an illustration, we here show an example of application for wake vortices in ground effects (IGE), see Fig. 15. As the ground is here taken flat, there is no need to solve a boundary integral equation for the panels strengths: by symmetry, those are directly obtained from the slip velocity evaluated at the wall. The problem is here periodic in x, and of extend $L_x = b_0$. Initially, the vortices are low order algebraic vortices (with $\sigma/b_0 = 0.05$) and are placed at height b_0. The discretization is $h/L_x = 1/64$. The simulation is a DNS at $Re = \Gamma_0/\nu = 5000$. It was run using the VIC-PFMM on 4 processors. The VIC grid grew from $64 \times 340 \times 92$ to $64 \times 390 \times 130$ (3.2 million) and the number of particles from 0.20 to 1.6 million. We see that short-wave instabilities develop on the secondary vortices produced at the ground. This results in a complex flow that will enhance the demise of the primary vortices. Longer extent simulations, also at high Reynolds number and using LES, are ongoing work.

8. Conclusions

This paper was aimed at presenting the Lagrangian vortex methods (mainly particle methods) for solving incompressible unsteady flows, including the recent developments: particle redistribution schemes, diffusion schemes, relaxation (projection) schemes, efficient velocity solvers (fast multipole method, vortex-in-cell method, combined method) and the efficient implementations on parallel computers.

The emphasis was on their application to the simulation of wing/aircraft trailing wake vortices. Various illustrative examples were considered and detailed: in 2-D and in 3-D, for quasi-inviscid simulations and for viscous flow simulations (using DNS and LES approaches; also a simplified RANS approach).

The main conclusion is that the modern particle methods are able to efficiently and accurately treat all types of unsteady convection-diffusion equations (also with source terms). They should be considered as mature and competitive numerical methods: methods that can be used for a wide variety of investigations: DNS, LES and unsteady RANS. The main advantage of Lagrangian methods is the fact that they have negligible dispersion error: they convect very well. This feature is still retained in the vortex-in-cell method, as the convection step is still Lagrangian.

In the field of trailing wake vortices, the methods have already been used with success for detailed studies: wake roll-up, global vortex tube dynamics, 3-D instabilities in vortex systems (also their saturation and the complex interactions/reconnections of vortex elements), the generated turbulence and the decay of the vortex system. The method is now also being applied to investigations of vortices interacting with the ground.

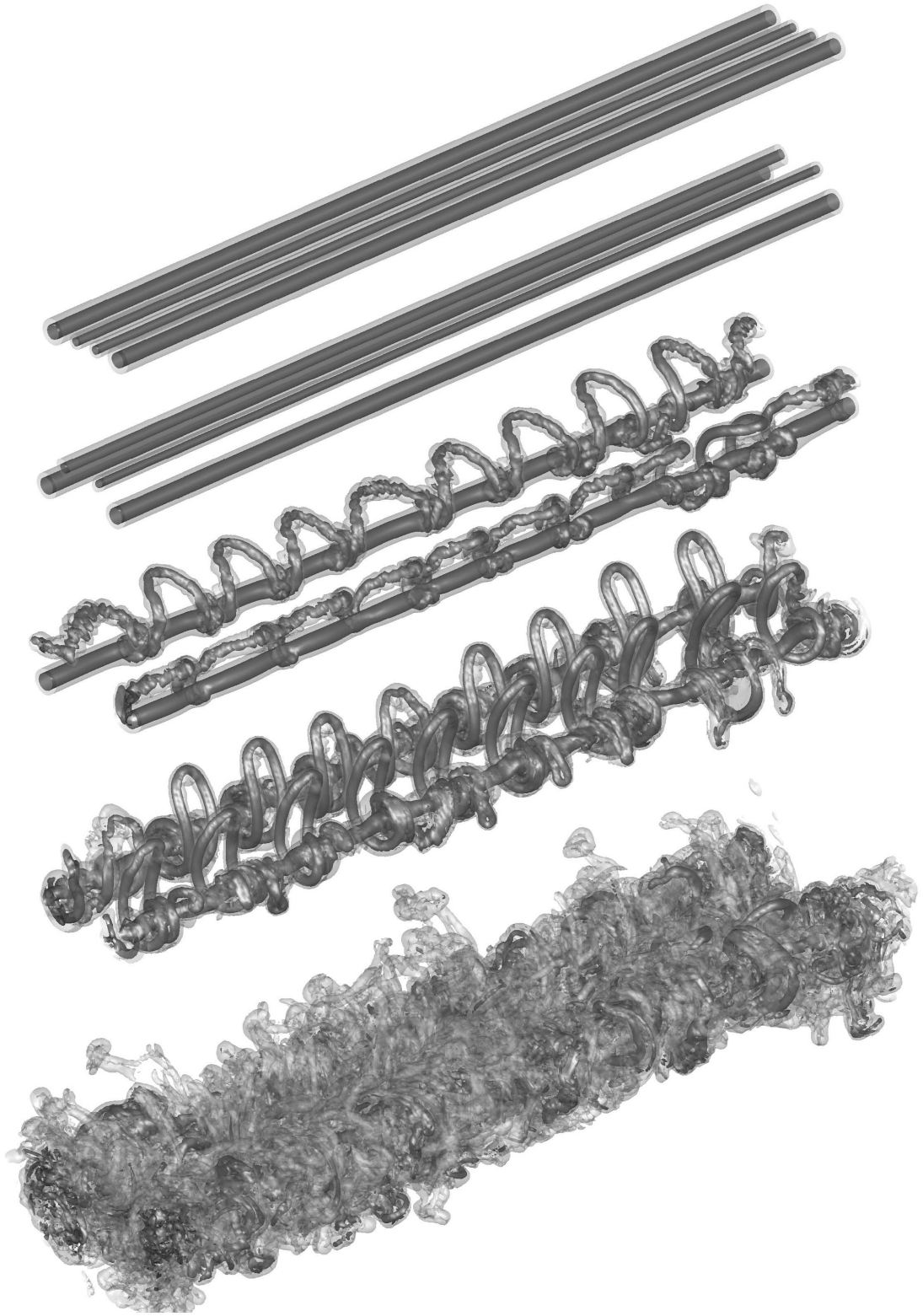

Fig. 13. Evolution of the four vortex system over a long domain. Iso-surfaces of vorticity modulus shown are $|\boldsymbol{\omega}|b_1^2/\Gamma_1 = 10.0$ (high opacity) and 2.0 (low opacity). Times are $\tau = 0.0$, 0.52, 1.06, 1.16 and 1.58.

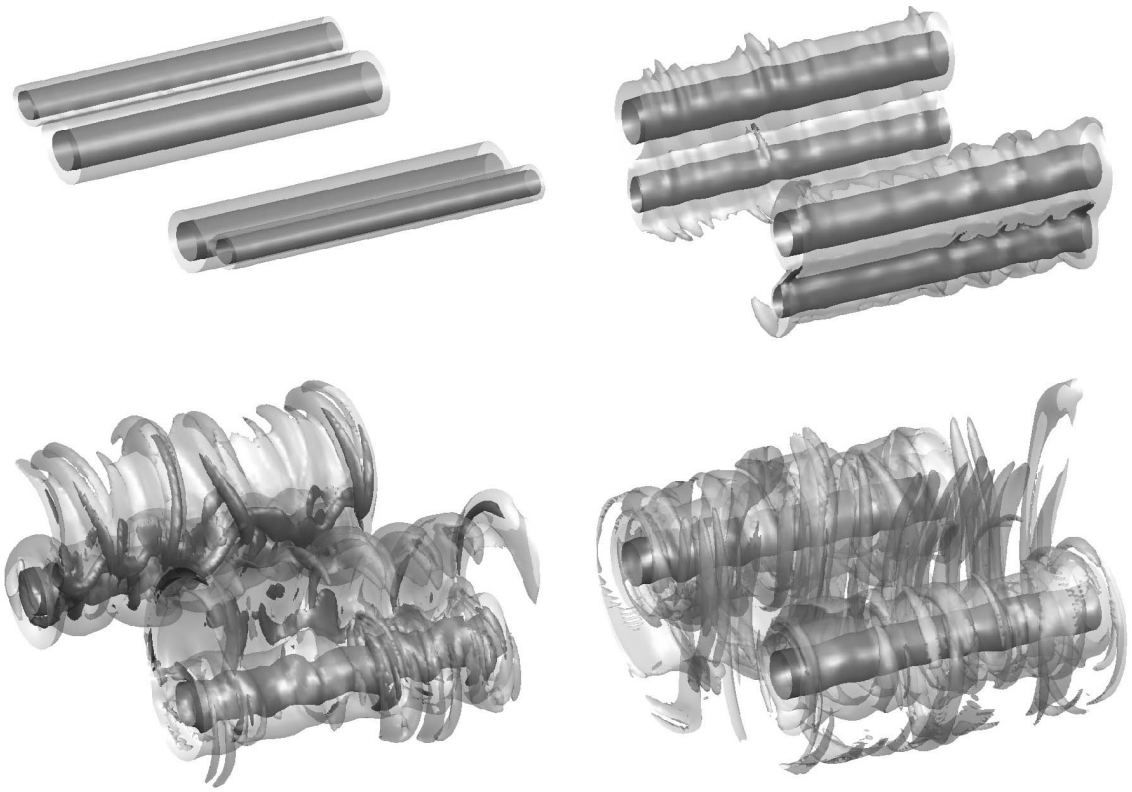

Fig. 14. Evolution of a co-rotating four vortex system. Iso-surfaces of vorticity modulus shown are $|\boldsymbol{\omega}|b_1^2/\Gamma_1 = 25.0$ (high opacity) and 5.0 (low opacity). Times are $\tau = 0.30$, 0.61, 0.91 and 1.21.

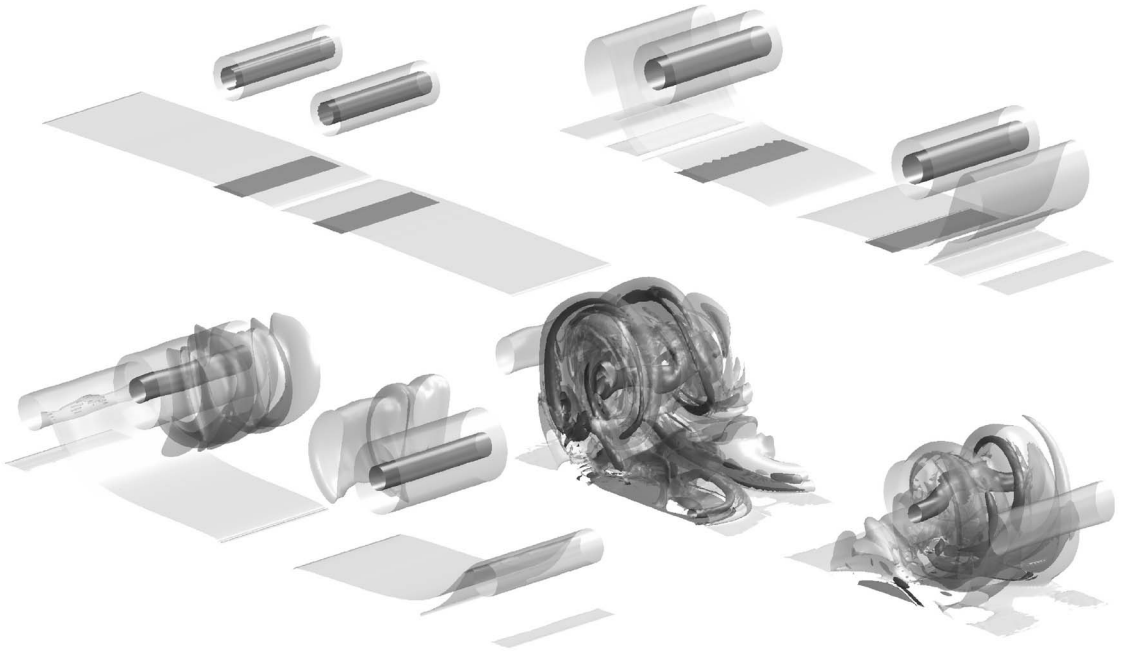

Fig. 15. Example of wake vortices in ground effects. Iso-surfaces of vorticity modulus shown are $|\boldsymbol{\omega}|b_0^2/\Gamma_0 = 10.0$ (high opacity) and 1.0 (low opacity). Times are $\tau = 0.0$, 1.6, 3.2 and 4.0

Acknowledgements

L. Dufresne was also funded under a postdoctoral fellowship from NSERC, Canada. The data on the SWIM experiments (made by NLR as part of the C-Wake project) were kindly provided by A. de Bruin of NLR. Part of the paper writing was also funded by the EC thematic network "WakeNet2-Europe" (contract G4RT-CT-2002-05115).

References

[1] G.-H. Cottet, P.D. Koumoutsakos, Vortex Methods, Theory and Practice, Cambridge Univ. Press, Cambridge, UK, 2000.
[2] G.S. Winckelmans, Vortex methods, in: E. Stein, R. de Borst, Th.J.R. Hughes (Eds.), The Encyclopedia of Computational Mechanics, vol. 3, John Wiley & Sons, October 2004.
[3] P.G. Saffman, Vortex Dynamics, Cambridge Univ. Press, Cambridge, UK, 1992.
[4] G.S. Winckelmans, A. Leonard, Contributions to vortex particle methods for the computation of three-dimensional incompressible unsteady flows, J. Comput. Phys. 109 (2) (1993) 247–273.
[5] A. Leonard, Vortex methods for flow simulation, J. Comput. Phys. 37 (1980) 289–335.
[6] A. Leonard, Computing three-dimensional incompressible flows with vortex elements, Annu. Rev. Fluid Mech. 17 (1985) 523–559.
[7] G.S. Winckelmans, Topics in vortex methods for the computation of three- and two-dimensional incompressible unsteady flows, PhD thesis, Graduate Aeronautical Laboratories, California Institute of Technology (Advisor A. Leonard), 1989 (http://etd.caltech.edu).
[8] D. Fabre, L. Jacquin, A. Loof, Optimal perturbations in a four-vortex aircraft wake in counter-rotating configuration, J. Fluid Mech. 451 (2002) 319–328.
[9] L. Jacquin, D. Fabre, D. Sipp, V. Theofilis, H. Vollmers, Instability and unsteadiness of aircraft wake vortices, Aerosp. Sci. Tech. 7 (2003) 577–593.
[10] J.M. Ortega, R.L. Bristol, Ó. Savas, Experimental study of the instability of unequal-strength counter-rotating vortex pairs, J. Fluid Mech. 474 (2003) 35–84.
[11] P. Degond, S. Mas-Gallic, The weighted particle method for convection–diffusion equations, Math. Comput. 53 (1989) 485–526.
[12] J.-P. Choquin, S. Huberson, Particle simulation of viscous flow, Comput. Fluids 17 (2) (1989) 397–410.
[13] G.-H. Cottet, S. Mas-Gallic, A particle method to solve the Navier–Stokes system, Numer. Math. 57 (1990) 805–827.
[14] G.-H. Cottet, Artificial viscosity models for vortex and particle methods, J. Comput. Phys. 127 (1996) 299–308.
[15] A.C. de Bruin, F.L.A. Ganzevles, Data analysis of wake survey tests behind SWIM model in DNW-LST and DNW-LLF windtunnels, C-Wake project, NLR-TR-2001-201, 2001.
[16] P.R. Owen, The decay of a turbulent trailing vortex, Aeronaut. Q. 21 (1970) 69–78.
[17] M.I. Yaras, Numerical simulations of aircraft wake-vortex dynamics in non-uniform windshear and ground proximity, AIAA paper 2002-0940, 2002.
[18] P. Ploumhans, G.S. Winckelmans, Vortex methods for high-resolution simulations of viscous flow past bluff bodies of general geometry, J. Comput. Phys. 165 (2000) 354–406.
[19] J.E. Barnes, P. Hut, A hierarchical $\mathcal{O}(N \log N)$ force-calculation algorithm, Nature 324 (1986) 446–449.
[20] L. Greengard, V. Rohklin, A fast algorithm for particle simulations, J. Comput. Phys. 73 (1987) 325–348.
[21] J.K. Salmon, M. Warren, Skeletons from the treecode closet, J. Comput. Phys. 111 (1994) 136–155.
[22] J.K. Salmon, M. Warren, G. Winckelmans, Fast parallel tree codes for gravitational and fluid dynamical N-body problems, Internat. J. Supercomput. Appl. High Performance Comput. 8 (2) (1994) 129–142.
[23] J.P. Christiansen, Numerical solution of hydrodynamics by the method of point vortices, J. Comput. Phys. 13 (1973) 363–379.
[24] G.-H. Cottet, B. Michaux, S. Ossia, G. Vanderlinden, A comparison of spectral and vortex methods in three-dimensional incompressible flows, J. Comput. Phys. 175 (2002) 702–712.
[25] G.-H. Cottet, P. Poncet, Particle methods for Direct Numerical Simulations of three-dimensional wakes, J. Turbulence 3 (028) (2003) 1–9 (http://jot.iop.org/).
[26] P. Koumoutsakos, A. Leonard, F. Pépin, Boundary conditions for viscous vortex methods, J. Comput. Phys. 113 (1994) 52–56.
[27] P. Koumoutsakos, A. Leonard, High resolution simulations of the flow around an impulsively started cylinder using vortex methods, J. Fluid Mech. 296 (1995) 1–38.
[28] P. Koumoutsakos, D. Shiels, Simulations of the viscous flow normal to an impulsively started and uniformly accelerated flat plate, J. Fluid Mech. 328 (1996) 177–226.
[29] P. Ploumhans, G.S. Winckelmans, J.K. Salmon, A. Leonard, M.S. Warren, Vortex methods for direct numerical simulation of three-dimensional bluff body flows: Application to the sphere at $Re = 300$, 500 and 1000, J. Comput. Phys. 178 (2002) 427–463.
[30] G.-H. Cottet, P. Poncet, Advances in direct numerical simulations of 3D wall-bounded flows by Vortex-in-Cell methods, J. Comput. Phys. 193 (2004) 136–158.
[31] P. Poncet, Vanishing of mode B in the wake behind a rotating circular cylinder, Phys. Fluids 14 (6) (2002) 2021.
[32] G.-H. Cottet, P.D. Koumoutsakos, M.L. Ould-Sahili, Vortex methods with spatially varying cores, J. Comput. Phys. 162 (2000) 164–185.
[33] G. Daeninck, P. Ploumhans, G.S. Winckelmans, Simulation of three-dimensional bluff-body flows using vortex methods: from direct numerical simulation towards large-eddy simulation modelling, J. Turbulence 3 (043) (2003) (http://jot.iop.org/).
[34] M.L. Ould-Salihi, G.-H. Cottet, M. El Hamraoui, Blending finite-difference and vortex methods for incompressible flow computations, SIAM J. Sci. Comput. 22 (5) (2000) 1655–1674.
[35] P.A. Raviart, An analysis of particle methods, in: Numerical Methods in Fluid Dynamics, in: Lecture Notes in Math. Ser., vol. 1127, Springer-Verlag, Berlin/New York, 1983, pp. 243–324.